WAVELENGTH REUSE IN UWB-OVER-FIBER NETWORKS

By

Wentao Cui

Thesis submitted to the
Faculty of Graduate and Postdoctoral Studies
In partial fulfillment of the requirements of
Master of Applied Science

Ottawa-Carleton Institute of Electrical and Computer Engineering
School of Electrical Engineering and Computer Science
University of Ottawa

ACKNOWLEDGEMENTS

First of all, I would like to express my sincere gratitude to my supervisor, Professor Jianping Yao, for providing me with strong academic atmosphere, state-of-the-art research facilities and valuable guidance. His enthusiastic and rigorous attitude towards scientific research inspires me. His profound knowledge enlightens me on my research and learning. His encouragement supports me to overcome frustrations. Without the help and patience from my supervisor, I would never finish these research works.

I would also like to appreciate the present and former colleagues in the Microwave Photonics Research Laboratory: Shilong Pan, Chao Wang, Ming Li, Muguang Wang, Xihua Zou, Wangzhe Li, Tong Shao, Weilin Liu, Weifeng Zhang, Liang Gao, Hiva Shahoei, Jiejun Zhang, Fanqi Kong, Yang Chen, Xiang Chen and Yinqing Pei. Their strong supports and helpful discussions have greatly improved my research work. Their friendship and encouragement have made my two years' experience in Canada memorable and meaningful.

Finally I would like to thank my parents for their immortal love and greatest support over my life. I would express my sincere love to my beloved family.

LIST OF PUBLICATIONS

[1] W. Cui, T. Shao, and J. P. Yao, "Wavelength reuse in a UWB over fiber system based on PM-IM conversion and destructive interferencing," *IEEE/OSA J. Lightw. Technol.*, vol. 31, no. 17, pp. 2904-2912, Sep. 2013.

[2] W. Cui, T. Shao, and J. P. Yao, "Wavelength reuse in a UWB over WDM-PON based on injection locking of a Fabry–Pérot laser diode and polarization multiplexing," *IEEE/OSA J. Lightw. Technol.*, accepted.

TABLE OF CONTENTS

ABSTRACT

Wavelength reuse techniques for bidirectional ultra-wide band (UWB) over fiber (UWBoF) networks are presented. The downstream optical signal from the central station (CS) is reused for upstream data transmission with the original data erased at the base station (BS). Two wavelength reuse schemes for the generation of a clear optical carrier at the BS are theoretically analyzed and experimentally demonstrated. In the first scheme, the wavelength reuse is based on phase-modulation to intensity-modulation (PM-IM) conversion and destructive interferencing using a polarization modulator (PolM) and a fiber Bragg grating (FBG). A theoretical analysis is performed which is verified by an experiment. In the second scheme, the wavelength reuse is based on injection locking of a Fabry–Pérot laser diode (FP-LD) and polarization multiplexing. The UWB injection signal contributes to better BERs of both downstream and upstream services and a lower power penalty cause by the wavelength reuse of the whole system than the baseband signal. A bidirectional point-to-point transmission of over a 25-km single-mode fiber (SMF) using a single wavelength from the CS in each scheme is demonstrated.

Chapter 1

Introduction

1.1 Background review

For future wireless local-area network (WLAN) and wireless personal-area network (WPAN) applications, it is generally required that the networks have the properties such as low-complexity, low-cost, low-power consumption and high-data-rate wireless connectivity [1]. Due to the very limited spectrum resources available below 10 GHz, the potential of these networks is restricted by the reality of radio system engineering [2]. To meet the increasing demand for high data rate transmission, ultra-wideband (UWB), which shares the spectrum with the existing radio communications systems, is regarded as a promising solution for future wireless access networks [1, 3-5]. UWB impulse technology has been around for a few decades and has been applied mainly to radar systems [6-18]. Recently, its application to broadband wireless communications has been extensively investigated. In 2002, the US Federal Communications Commission (FCC) approved unlicensed use of a spectrum from 3.1 to 10.6 GHz centered around 7 GHz with a spectrum width of 7.5 GHz for UWB indoor communication

devices [19]. The power spectral density (PSD) is limited to 41.3 dBm/MHz [19]. According to the definition in Part 15 of the FCC regulations, a UWB impulse signal should have a fractional bandwidth larger than 20% or a 10-dB bandwidth of at least 500 MHz [6].

UWB is considered a promising solution for short-range high-throughput wireless communications and sensor networks due to its intrinsic properties, such as immunity to multipath fading, extremely short time duration, being carrier free, and having low duty cycle, wide bandwidth, and low power spectral density [1, 3, 4, 20-24]. Because of the low PSD, UWB communications can co-exist with other conventional wireless communications with negligible interferences [1], but the transmission distance is limited to a few to tens of meters [6, 20]. To extend the area of coverage and integrate UWB services into fixed wired or wireless communications networks, a solution is to distribute UWB signals over optical fiber, or UWB-over-fiber (UWBoF) [6, 20]. In a typical UWBoF system for broadband indoor wireless access, the UWB signals are generated in the central station (CS) and distributed to the access points (APs) or BSs through the optical fiber [20].

On the other hand, fixed fiber deployments for fiber to the home (FTTH) services are increasing. Passive optical network (PON) technology is the leading FTTH technology, including Gigabit PON (GPON) and Ethernet PON (EPON), both are based on time-division multiple access (TDMA), providing services to N users by use of passive 1:*N* power splitters with an aggregate bit rate. These techniques, however, are regarded to not be able to keep up with the requirements for future access networks regarding aggregated bandwidth, attainable reach and allowable power budget [25-28]. These problems can be mitigated by assigning an individual wavelength to each optical network unit (ONU). The architecture, referred to as a wavelength division multiplexed passive optical network (WDM-PON), is attractive due to the advantages, such as increased per ONU bandwidth, reduced optical splitting loss, point-to-point connectivity, protocol agnosticism, bit-rate transparency, large scalability, and high flexibility [29, 30]. Consequently, there is a worldwide consensus that the current TDMA-PON would evolve towards WDM-PON [27]. Under this background, it is of great interest to integrate a UWBoF system into a WDM-PON network [2, 31, 32].

In a WDM-PON, despite all these advantages, multiple light sources and wavelength selective components with high wavelength precision are needed, which may increase the system complexity and cost and in turn render

WDM-PON not yet competitive with other optical access network solutions [27]. To make the UWB over WDM-PON systems practical for future commercial deployment, it is desirable to simplify the operation, ease the maintenance and reduce the cost. Therefore, the generation of low-cost UWB impulse signals in the optical line terminal (OLT) and the construction of simple ONUs are two key technologies necessary to implement a UWB over WDM-PON system [33] and are to be discussed as follows.

To implement the generation of low-cost UWB impulse signals in the OLT and distribute UWB signals over the optical fiber, it is highly desirable to directly generate UWB signals in the optical domain due to the many superior advantages, such as no need for extra electrical-to-optical conversion, light weight, small size, large tunability, and immunity to electromagnetic interference [20]. Previously, Yao *et al.* has summarized and classified photonic generation of UWB signals into three categories [6, 20]: 1) UWB pulse generation based on phase modulation to intensity modulation (PM-IM) conversion where the PM-IM conversion can be implemented using a frequency discriminator or a dispersive device in the optical domain [20, 34-36]; 2) UWB pulse generation using a photonic microwave delay-line filter; a two- or three-tap microwave filter with coefficients of (1, -1) or (1, -2, 1) can operate as a first- or second-order difference on a Gaussian pulse,

which can be approximated as a first- or second-order derivative [37, 38]; 3) UWB pulse generation based on optical spectral shaping and dispersion-induced frequency-to-time mapping; the spectrum of an ultrashort pulse is shaped by an optical filter into that corresponding to a UWB monocycle or doublet and then converted from spectral domain to temporal domain through a dispersive device, which is called frequency-to-time mapping [39, 40]. In the work presented in this thesis, photonic generation of UWB signals is realized through the first method and will be discussed in details in Chapter 3.

Recently, new techniques to implement photonic generation of UWB signals have been proposed and demonstrated. Based on the summary by Yao *et al.* in [6] and [20], a modified classification is made for these techniques and photonic generation UWB signals are classified into four categories: 1) PM-IM conversion, 2) photonic microwave bandpass filters, 3) optical spectral shaping and dispersion-induced frequency-to-time mapping, and 4) excitation of relaxation oscillations of a semiconductor laser. A detailed discussion of these techniques is given in Chapter 2.

In addition, to make UWB over WDM-PON systems practical for future commercial deployment, it is necessary to minimize the construction and

maintenance cost of the ONUs and shift the complex parts and expensive devices of the system architecture to the OLT to maximize its centralized functions [41]. In this situation, wavelength reuse has been proposed as an effective solution to reduce the cost as well as to realize a "colorless" ONU in which the upstream service shares the same wavelength channel as that of the downstream service [29, 42-45]. In a wavelength reused WDM-PON, the colorless ONUs are equally equipped with low-cost and stable receivers for downstream signals and transmitters for upstream signals. Such property reduces the construction and maintenance cost of the ONUs, because an identical backup ONU can directly replace the malfunctioning one. Without colorless ONUs, light sources with tunable property or different wavelengths will be needed in the backup ONUs. Among the various wavelength reuse schemes, injection locking of a Fabry-Pérot laser diode (FP-LD) [46-49], gain-saturation of a reflective semiconductor optical amplifier (RSOA) [50-53], and optical carrier separation for uplink connection [54-57] have been considered three major solutions and have been widely investigated. At an FP-LD based ONU, when the FP-LD is injection locked, it will lase at the same wavelength as the injected downstream signal with the original data largely suppressed, thus enables the output wavelength to be re-used for upstream data transmission [25]. In an RSOA based ONU, an RSOA with a relatively low input saturation power is employed, when the input power of the

downstream signal is sufficiently high, the RSOA will work at the gain saturation region and the downstream data will be erased. The output light can be reused to be intensity re-modulated by a signal for upstream transmission [42, 43]. In the third method, optical carriers are separated and re-utilized for uplink transmission [54-57]. In each channel, through the combination of double sideband modulation and optical carrier suppression, only one wavelength and the generated sidebands are needed and used as the optical carriers for downstream and upstream transmissions. Some of these optical carriers are used as the downstream carriers while the others are for the upstream transmission, which means separated optical carriers are employed for bidirectional transmission.

However, the performance of a WDM-PON utilizing either of these three wavelength reuse techniques is limited due to the intrinsic limitation of these three methods. 1) For the scheme using injection locking of an FP-LD, the commonly utilized downstream injection optical signal is a baseband signal. The limitation of such an injection locking method is that the performance of the upstream signal is sensitive to the modulation depth or extinction ratio (ER) of the downstream signal. When the modulation depth of the downstream baseband signal increases, the injection-locked optical carrier at the output of the FP-LD is severely degraded and is not suitable for upstream data re-modulation. Therefore, there is an obvious

tradeoff between the ER of the downstream signal and the performance of the upstream signal transmission. 2) Similarly, the major limitation of the scheme using an RSOA is that a tradeoff between the ER of the downstream and the performance of the upstream signal transmission always exists. 3) For the scheme using separated optical carriers, the utilization efficiency of the optical carriers is low since different optical carriers are assigned for bidirectional transmission. In addition, when broader signal bandwidth is required, the channel spacing of a WDM-PON has to be increased to ensure non-overlapping assigned frequency bands for bidirectional transmission. Therefore, wavelength reuse techniques that can reduce or even eliminate such limitations are highly desirable and of great interest to improve the transmission performance of a WDM-PON.

In this thesis, we propose two wavelength reuse techniques to improve the transmission performance and simplify the system architecture of a WDM-PON, both with a centralized OLT and simple ONUs.

In the first technique, a novel wavelength reuse scheme based on PM-IM conversion and destructive interferencing using a polarization modulator (PolM) and a fiber Bragg grating (FBG) in a UWBoF system is proposed and experimentally demonstrated. In the proposed scheme, a PolM and an FBG in the

CS are used to generate two intensity-modulated UWB impulse signals along two orthogonal states of polarization (SOPs) based on PM-IM conversion. The downstream UWB signal is sent to a base station (BS) over an optical fiber. At the BS, when the principal axis of the polarizer is aligned with one of the two orthogonal SOPs, the downstream UWB signal is received and detected. When the principal axis of the polarizer is oriented at a special angle to one of the two orthogonal SOPs, the two projected optical signals on the principle axis of the polarizer would lead to the generation of two complementary intensity-modulated UWB signals and cancel each other, then a clear optical carrier without intensity modulation is generated, which is then reused for upstream UWB data transmission. A theoretical analysis is performed which is verified by an experiment. A bidirectional point-to-point transmission of 1.25 Gb/s UWB signal over 25-km single-mode fiber (SMF) using a single light source from the CS is demonstrated. The receiver sensitivity and the bit error rate (BER) performance for both downstream and upstream transmissions are measured. The proposed technique is theoretically analyzed and experimentally demonstrated in Chapter 3.

In the second technique, wavelength reuse in a symmetric UWB over WDM-PON based on injection locking of an FP-LD and polarization multiplexing is proposed and experimentally demonstrated. In the proposed scheme, the downstream UWB

signal and baseband signal are generated and polarization multiplexed in the CS and sent to the BS over an optical fiber. At the BS, one of the downstream signals is selected to injection lock the FP-LD. It is demonstrated theoretically and experimentally that the upstream service performance is less sensitive to the modulation depth of the downstream UWB signal than the baseband signal, and the use of the downstream UWB signal as the injection signal would contribute to a better transmission performance for both the downstream and upstream services. Thus, the downstream UWB signal is selected as the injection signal. An experiment is performed. When the FP-LD is injection locked by a downstream UWB signal, a clear optical carrier is generated which is reused for upstream UWB and baseband transmission. A bidirectional point-to-point transmission of 1.25 Gb/s UWB signal and 10 Gb/s baseband signal over 25-km SMF using a single wavelength is demonstrated. The BER performance and the eye diagrams for both downstream and upstream transmission are measured. A theoretical analysis as well as a verification experiment is presented for the proposed technique in Chapter 4.

Briefly speaking, the first experiment emphasizes the photonic generation of UWB signals in the CS and the wavelength reuse process in the BS without any active component. The second experiment deals with the provision of baseband

and UWB services in a single wavelength channel, with enhanced receiver sensitivities for bidirectional transmission. Each scheme has exclusive advantages over conventional wavelength reuse schemes.

It should be noted that, although photonic generation of UWB signals and wavelength reuse techniques are regarded as two key technologies for the implementation of a UWB over WDM-PON, which are also applicable to a UWBoF system. This is because the employment of these techniques is to enhance the transmission performance while simplifying the system architecture, which is also highly desirable for a UWBoF system.

1.2 Investigated issues and contributions

In this thesis, two wavelength reuse techniques are proposed and experimentally verified to implement bidirectional UWBoF networks. The purpose of the research work is to present novel and effective wavelength reuse schemes that can overcome the limitations of conventional wavelength reuse techniques for radio over fiber and WDM-PON applications, which have been discussed in Chapter 1.1. The main investigated issues and contributions are presented as follows.

(1) In the first work, the proposed wavelength reuse scheme for a UWBoF system presents a detailed theoretical analysis of 1) photonic generation of UWB impulse signals based on PM-IM conversion using an FBG based frequency discriminator and 2) wavelength reuse for upstream transmission based on destructive interferencing. The proposed wavelength reuse scheme has the following advantages. First, a clear optical carrier without intensity modulation for upstream transmission can be generated at the BS, and the erasing process of the downstream data is independent of the modulation depth and data rate of the downstream signal. For the schemes using a separated optical carrier, part of the carriers is not modulated but intended for upstream modulation, the modulation efficiency is thus relatively low. In addition, the demodulation of the subcarrier multiplexed downstream signal at the BS is complicated and costly. In the

proposed scheme, the UWB signal is directly generated and modulated on the optical carrier in the optical domain at the CS. At the BS, the upstream service shares exactly the same carrier as the downstream one, which means the optical carrier is completely used for both downstream and upstream services. For the conventional schemes using baseband signal injected FP-LDs and RSOAs, there is a tradeoff between the ERs of the downstream and upstream signals, while in the proposed scheme the modulation depth of the downstream signal has negligible impact on the performance of the upstream service. Second, the wavelength reuse at the BS of the proposed system is based on adjusting the principal axis of the polarizer, no active element is utilized. Therefore, there are no additional noise and nonlinearity imposed on the generated optical carrier. This property also contributes to a much clearer optical carrier for upstream transmission. A power penalty due to the wavelength reuse is measured to be as low as 0.2 dB. Detailed descriptions of this work are presented in Chapter 3.

(2) In the second work, a comparative study is performed in which the injection locking using a baseband and a UWB downstream signal is considered to evaluate the performance of injection locking of the FP-LD. For both signals having an identical optical injection power and identical electrical modulation power, injection locking using a UWB signal shows a clear advantage over the use of a

baseband signal. Theoretical analysis is presented to explain the superior property of UWB signals for injection locking. It is also experimentally demonstrated that the injection locking of an FP-LD using a UWB signal would make the upstream service performance is less sensitive to the ER of the downstream signal than the baseband signal, and the use of the downstream UWB signal as the injection signal would contribute to a better transmission performance for both downstream and upstream services. The proposed wavelength reuse scheme for the UWB over WDM-PON system has the following advantage. When the UWB signal and the baseband signal have the same injected optical power, the UWB signal can have a higher electrical modulation power than that of the baseband signal, without obvious negative impact on the performance of the upstream signal. This in turn contributes to a better receiver sensitivity of the downstream UWB service. It is true that there is a tradeoff between the ERs of the downstream and upstream signals for the case of both UWB and baseband injected signals; however, the utilization of the UWB signal as the injected signal enables the system with a higher tolerance against the power penalty introduced by a relatively higher ER of the downstream signal. Therefore, better performances for both downstream and upstream services of the proposed UWB over WDM-PON can be obtained thanks to this property. The power penalty due to wavelength reuse is measured to be as

low as 0.2 dB. In Chapter 4, a detailed theoretical explanation as well as experimental results of the proposed wavelength reuse scheme is presented.

1.3 Organization

This thesis consists of five chapters. In Chapter 1, a background review regarding the necessity of UWBoF networks and the evolution of current TDMA-PON towards WDM-PON is presented. Two key technologies and corresponding solutions to implement UWB over WDM-PON are discussed. A brief introduction of the research work in this thesis is also given. The investigated issues and contributions of the research work are introduced. In Chapter 2, state-of-the-art UWBoF networks techniques are reviewed. Architecture of UWBoF system as well as main approaches for photonic generation of UWB signals is introduced. Techniques to realize simultaneous provision of wired and wireless services and wavelength reuse in a UWB over WDM-PON are also introduced and compared. In Chapter 3, a bidirectional UWBoF system based on PM-IM conversion and destructive interferencing is demonstrated. The mathematical derivation of photonic generation and detection of UWB impulse signals as well as the wavelength reuse process is given. The principles of corresponding processes are also theoretically explained. The results of the verification experiment are presented. In Chapter 4, a bidirectional UWB over WDM-PON based on injection locking of an FP-LD and polarization multiplexing is theoretically and experimentally presented. A comparative study is also performed in which the injection locking using a baseband and a UWB downstream signal is considered

to evaluate the performance of injection locking of the FP-LD. Finally, conclusions of this thesis as well as the future works succeeding this research work are given.

Chapter 2

Review of UWB-over-fiber networks

2.1 UWB-over-fiber system

Based on the definition by the US FCC, the frequency band assigned to UWB indoor communications systems extends from 3.1 to 10.6 GHz, with a bandwidth of 7.5 GHz centered around 7 GHz. The PSD is limited to -41.3 dBm/MHz [19]. Due to the low PSD, UWB communications can co-exist with other conventional wireless communications with negligible interferences, but the transmission distance is limited to a few to tens of meters. Such a short-range communications network can only operate in a stand-alone mode in an indoor environment [6]. To enable seamless UWB service across different networks and achieve high-data-rate access whenever and wherever there is a need, UWB service should be distributed through optical fiber and integrated into fixed wide-area wired or wireless networks [20]. Under this circumstance, UWBoF technique is proposed and regarded as a promising solution.

Similarly to the architecture of a radio over fiber system [58-61], for a UWBoF system, the design principle is to minimize the cost and complexity of the APs or BSs and maximize the centralized function of the CS.

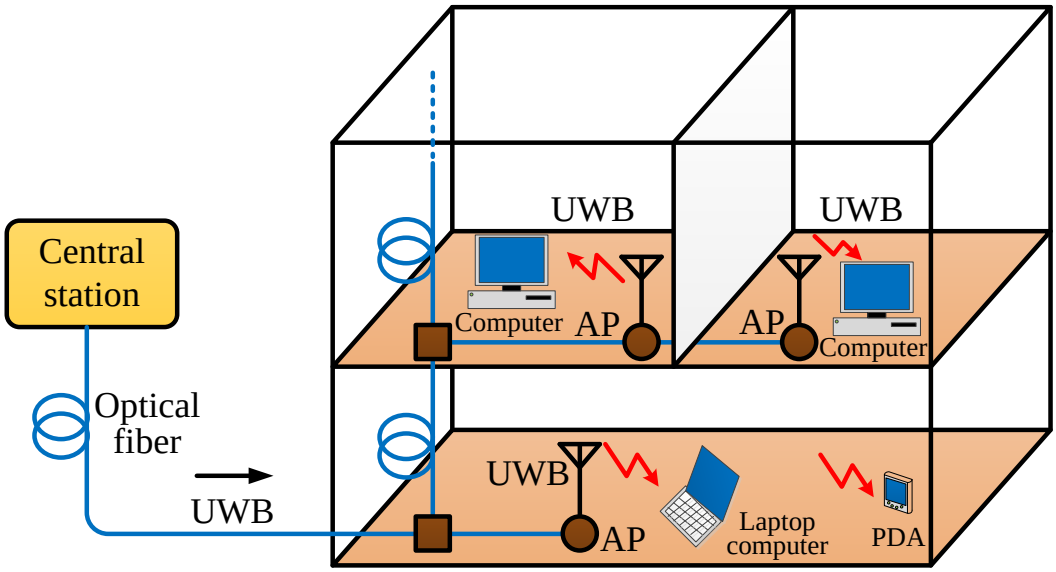

Fig. 2.1. A conceptual illustration of a UWBoF system for broadband indoor wireless access [20].

Fig. 2.1 shows a conceptual illustration of a UWBoF system for broadband indoor wireless access [20]. In the system, UWB signals are directly generated and encoded in the CS and distributed to the APs over optical fiber [6, 20]. At the APs, the UWB signals are converted into electrical domain from optical domain and radiated into free space [6]. The downstream wireless UWB signals are then received by the end users, such as computers and personal digital assistants

(PDAs). The upstream transmission of the UWBoF system would utilize a simple and mature wireless communication technique (such as a wireless local-area network) since relatively lower data rate is required for upstream transmission compared with the downstream service [6]. In this situation, the UWBoF system is operating in a hybrid mode where both the high data rate UWB technology and the low cost wireless communication technology are used [6]. However, it is also desirable to realize a symmetrical UWBoF system where both the downstream and upstream services are equipped with UWB technology, on condition that the system is of low cost and complexity. In this thesis, a simple and cost effective bidirectional UWBoF architecture is proposed and will be presented in Chapter 3 in detail.

2.2 UWB over WDM-PON: key technologies

As has been discussed in Chapter 1, when implementing a UWB over WDM-PON system, photonic generation of UWB impulse signals and wavelength reuse are two key technologies to enhance the system performance and reduce the cost. In this section, different proposed solutions of the two technologies are reviewed.

2.2.1 Photonic generation of UWB signals

It has been demonstrated extensively that UWB signals can be generated electrically. Among numerous proposed solutions, considering research interests have been taken in developing a UWB bandpass filter [62-65] and a microwave differentiator based UWB generator [66-68]. However, as has been discussed in Chapter 1, in a UWBoF system it is highly desirable that the UWB signals can be generated directly in the optical domain due to the many superior advantages, such as no need for extra electrical-to-optical conversion, light weight, small size, large tunability, and immunity to electromagnetic interference [20]. Since the emergence of the definition of UWBoF, photonic generation of UWB signals have been investigated extensively and numerous approaches have been proposed. Based on the summary by Yao *et al.* in [6] and [20], a modified classification is made for these approaches and photonic generation UWB signals are summarized

to be based on four categories: 1) PM-IM conversion; 2) photonic microwave bandpass filters; 3) optical spectral shaping and dispersion-induced frequency-to-time mapping; 4) excitation of relaxation oscillations of a semiconductor laser. In this section, detailed descriptions of these techniques are given as follows.

2.2.1.1 PM-IM conversion technique

Photonic generation of UWB signals based on PM-IM conversion can be implemented using a frequency discriminator or a dispersive device in the optical domain [20]. Fig. 2.2 shows the operating principle of PM-IM conversion based on a frequency discriminator or a dispersive device [20].

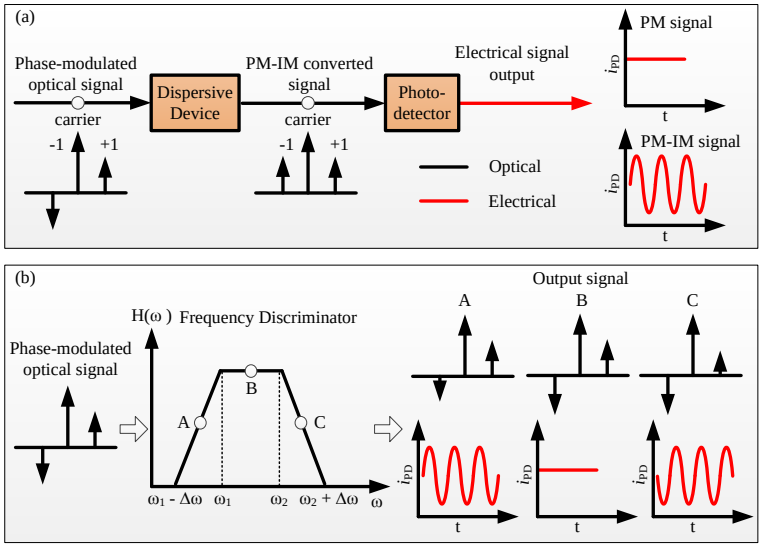

Fig. 2.2. A principle illustration of PM-IM conversion using (a) a dispersive device and (b) a frequency discriminator [20].

As is shown in Fig. 2.2(a), for a phase-modulated signal where the upper and lower first-order sidebands are out-of-phase. When conducting photo-detection, the output electrical signal only contains direct current (DC) component. A dispersive device here is used to introduce phase difference between the two first-order sidebands. Then the out-of-phase sidebands can be changed into the partially or totally in-phase ones. In this situation, the electrical signal after photo-detection will reveal the modulation information. In another word, PM-IM conversion is achieved through the utilization of this dispersive device. For a dispersive device with a quadratic phase response, the chromatic-dispersion-based PM – IM conversion with direct detection has a frequency response that is given by [20]

$$H_{PM-IM}(\omega_m) = \sin\left(\frac{1}{2} D_\omega \omega_m^2\right) \tag{2-1}$$

where D_ω is the dispersion parameter of the dispersive device and ω_m is the modulating frequency. The frequency response is a quasi-periodic function with a notch at DC. The first and the second notch of the frequency response forms a passband which can shape the spectrum of the input signal. For a Gaussian input

pulse, a Gaussian monocycle or doublet will be generated since the frequency components at DC is filtered out. Therefore, UWB impulses can be generated.

For a frequency discriminator, which is usually an optical filter, the magnitude relation of the lower and upper first-order sidebands will be changed by passing through the frequency discriminator, then the information on the phase is transferred to the magnitude after direction detection. In this way, PM-IM conversion can also be realized. For a linear frequency discriminator, the mathematical expression of the frequency response as well as the output signal is given in [6] and [20]

$$\left|H_d(j\omega)\right| = K\omega - K(\omega_1 - \Delta\omega) \qquad \left(\omega_1 - \Delta\omega \le \omega \le \omega_1\right) \tag{2-2}$$

where K is the slope of the filter ($K > 0$), ω is the optical frequency, ω_1 is the upper frequency limit of the linear region and $\Delta\omega$ is the detuning range of the linear region. The recovered radio-frequency (RF) signal after the filtering and direct detection is expressed as [20]

$$r(t) \sim 2PK^2\left(\omega_0 - \omega_1 + \Delta\omega\right)\beta_{PM} f'(t) \tag{2-3}$$

where P is the optical power at the input of the photodetector (PD), ω_0 is the frequency of the optical carrier, β_{PM} is the phase modulation index and $f'(t)$ is the first-order derivative of the modulation signal $f(t)$. From 2-3, we can conclude that the recovered signal is proportional to the first-order derivative of the modulation signal. If the modulation signal is a Gaussian pulse, the detected signal will be a Gaussian monocycle. Therefore, PM-IM conversion is implemented and UWB impulse signal can be generated.

Based on the above principle, numerous experimental schemes have been proposed and demonstrated [25, 34-36, 69-73].

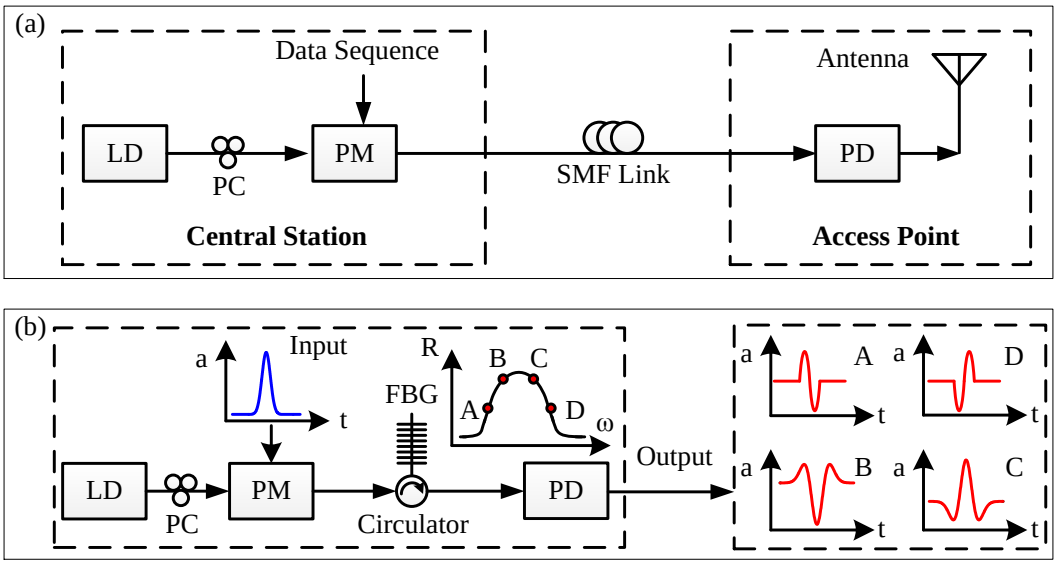

Fig. 2.3. Schematic diagrams of PM-IM conversion techniques for photonic generation of UWB signals using (a) a dispersive device [36] and (b) a frequency discriminator [34]. PC: polarization controller; LD: laser diode.

Fig. 2.3(a) shows the schematic diagram of PM-IM conversion technique for photonic generation of UWB signal using a dispersive device [36]. In this system, a continuous wave (CW) light emitted from an LD is phase-modulated by a data sequence which is a pseudorandom bit sequence (PRBS) Gaussian pulse train. The dispersive device in this system is a length of SMF which performs PM-IM conversion for the phase-modulated Gaussian pulse train. At the AP, the PM-IM converted signal is direct detected by the PD. Due to the bandpass character of the transmission system, the phase-modulated Gaussian pulse train is converted into an intensity-modulated Gaussian doublet pulse train, i.e. the UWB impulse signal. Then the electrical UWB signal is radiated into free space through the UWB antenna. The advantage of this system is that the UWB signal is optically generated through a simple architecture and distributed to the AP in the meantime. However, the optical generation and distribution is actually implemented through the same device. When the transmission distance is different, the frequency response of the system is different, which will in turn impact the spectrum shape of the generated UWB signal.

Fig. 2.3(b) shows the schematic diagram of PM-IM conversion technique for photonic generation of UWB signal using a frequency discriminator [34]. In this

system, an FBG with a proper Gaussian apodization is used as a frequency discriminator. As can be seen in the figure, the phase-modulated Gaussian impulse sequence is applied into the FBG to perform PM-IM conversion. By locating the optical carrier at the linear (point A and D) or quadrature slope (point B and C) of the FBG reflection spectrum, intensity-modulated Gaussian monocycle or doublet can be generated at the output of the PD. It should be noted that by locating the optical carrier at the opposite slopes of the reflection spectrum, UWB impulses with opposite polarities can be generated. As can be seen from the subset of Fig. 2.3(b), Gaussian monocycles with different polarities are generated at point A and D while Gaussian doublets with different polarities are generated at point B and C. Therefore, this system can implement pulse shape modulation and pulse polarity modulation by shifting the wavelength of the optical carrier [34].

2.2.1.2 Photonic microwave bandpass filter technique

Photonic generation of UWB signals based on photonic microwave filter has attracted considerable interest recently due to its advantages in advanced signal processing. To implement UWB impulse generation, a photonic microwave filter should have a passband from 3.1 GHz to 10.6 GHz to shape a Gaussian pulse to a Gaussian monocycle or a doublet and to simultaneously reduce the out-band noise

and interferences [2]. In [6] and [20], UWB signal generation based on photonic microwave delay-line filter is summarized. In [37, 38], UWB impulses are generated based on two- or three-tap photonic microwave delay-line filter, however, the employment of high-performance balanced PD would greatly increase the system cost [2]. In [74-77], balanced PD is eliminated for differential detection; however, the summation of time delayed intensity-modulated optical signals is realized through multiple light sources. In another word, system cost is increased by the laser array at the OLT; moreover, such system architecture is not compatible with that of a WDM-PON where only one wavelength is used in one channel. Recently, UWB signal generation solutions based on photonic microwave filters without expensive balanced PD or multiple laser sources have been proposed and experimentally demonstrated [2, 78-80].

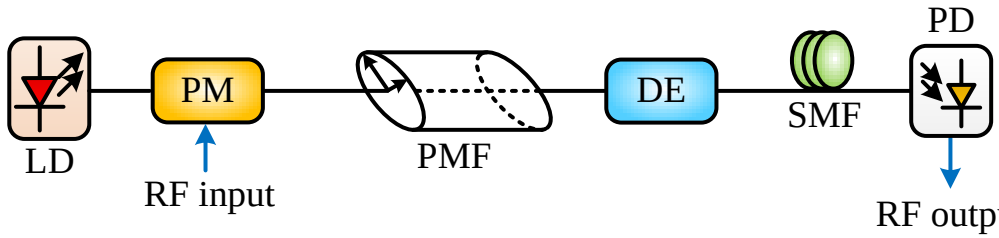

Fig. 2.4. Schematic diagram of a PM based photonic microwave filter [2]. PMF: polarization-maintaining fiber; DE: dispersive element.

Fig. 2.4 shows the schematic diagram of a PM based photonic microwave filter [2]. A linearly polarized CW light from an LD is phase-modulated by a PRBS Gaussian pulse train. The phase-modulated signal is then applied to a PMF based delay line with the extraordinary axis of the PM having an angle of $45°$ to the principal axes of the PMF. The PMF based delay line filter is a two-tap photonic microwave filter. The DE here is used to introduce large chromatic dispersion compared with that from the SMF transmission. The magnitude frequency response of the photonic microwave bandpass filter is written as [2]

$$\left|H(f)\right| = \underbrace{\left|\cos(\pi f \tau)\right|}_{|H_1(f)|} \cdot \underbrace{\left|\sin\left(\frac{\pi(\chi + DL)\lambda^2 f^2}{c}\right)\right|}_{H_2(f)} \tag{2-4}$$

where $\left|H_1(f)\right|$ and $\left|H_2(f)\right|$ are the magnitude frequency response of the PMF based low-pass and DE-SMF based bandpass photonic microwave filters, f is the frequency, τ denotes the differential group delay (DGD) introduced by the PMF to the two orthogonally polarized modes along the two principal axes, χ is the dispersion of the DE, D and L are the dispersion parameter and the length of the SMF respectively, λ is the wavelength of the optical carrier and c is the speed of light in vacuum. The multiplication of $\left|H_1(f)\right|$ and $\left|H_2(f)\right|$ results in a passband at UWB frequency band. The magnitude frequency response of the

system not only shape a Gaussian pulse train into a Gaussian monocycle or doublet train, but also have a good tolerance against the SMF induced dispersion. This is because the frequency at the first notch of the PMF-induced low-pass filter (LPF) is smaller than that at the second notch of the dispersion-induced bandpass filter. Thus, the upper bound of the filter is governed by the first notch determined by τ [2]. The proposed system not only eliminates the expensive multiple laser source and balanced PD, but also is independent of the SMF length in a large range.

2.2.1.3 Optical spectral-shaping and dispersion-induced frequency-to-time mapping technique

Due to the high limitation on the transmitted power density set by the FCC on the UWB signals, it is highly desirable that UWB impulses can be generated with the maximum utilization of the assigned frequency band and power limit in the meantime. Pulse-shaping technique that enables the maximum occupation of legally allowed transmission power is a very efficient and effective solution to enhance UWB performance [81]. The wideband spectrum of a sequence of ultrashort pulses is thus shaped into that of a Gaussian monocycle or doublet sequence. Then a dispersive device, which is usually a length of SMF or a linear chirped FBG, will serve as a real-time Fourier transformer to perform

frequency-to-time conversion. Various photonic generation UWB signals techniques based on spectrum shaping and frequency-to-time conversion have been proposed [39, 40, 81-83].

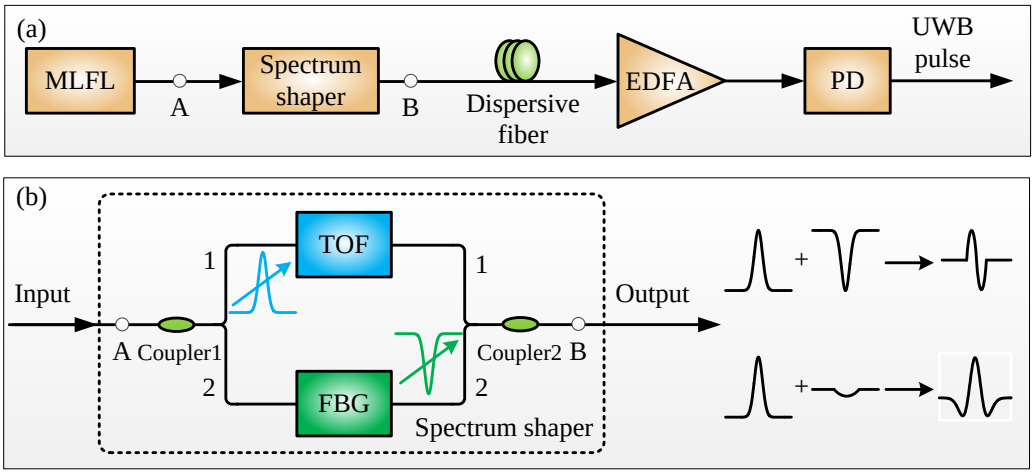

Fig. 2.5. (a) Schematic diagram of an all-fiber UWB signal generation system based on spectral shaping and dispersion-induced frequency-to-time mapping. (b) All-fiber spectrum shaper configuration. MLFL: mode-locked fiber laser; EDFA: erbium-doped fiber amplifier; TOF: tunable optical filter [40].

Fig. 2.5(a) shows the schematic diagram of an all-fiber UWB signal generation system based on spectral shaping and dispersion-induced frequency-to-time mapping. A sequence of ultrashort pulse train from a MLFL is spectrally shaped by an all optical spectrum shaper. The frequency response of the spectrum shaper is designed to shape a wideband spectrum into that corresponds to a Gaussian monocycle or a doublet. Then the spectrally shaped optical signal is sent to a

length of dispersive SMF to perform frequency-to-time mapping. The total chromatic dispersion must be properly determined according to the mapping relationship between the spectrum bandwidth and the temporal pulse width [40]. After the amplification at the EDFA and the optical to electrical conversion at the PD, a temporal Gaussian monocycle or doublet can be obtained. Fig. 2.5(b) shows the configuration of the all-fiber spectrum shaper. The input wideband optical pulse trains are divided into two paths, each of which passes through an optical filter to have its spectrum shaped according to the required spectrum shape. The ultrashort pulse train is filtered by an TOF in one path while the other one is transmitted through an FBG based filter. To generate a Gaussian monocycle train, the bandwidth and the absolute spectral peaks of the two filters should be identical. There should also be a proper difference between the center wavelengths of the two filters to introduce required time difference between the two temporal pulse trains after frequency-to-time conversion. To generate a Gaussian doublet train, the center wavelength of the two filters should be same. A redesigned FBG with a broader bandwidth is employed. The negative spectral peak of the FBG is decreased by tuning the coupling ratio of OC1. All these adjustments are to ensure that the generated Gaussian doublet meets the UWB spectrum requirement.

One drawback of this technique is that in addition to the UWB spectrum, there is a baseband spectral component, which is resulted from the wide Gaussian-like pedestal [40]. To eliminate such pedestal, new solution has been proposed by using balanced photodetection [81].

2.2.1.4 Excitation of relaxation oscillations of a semiconductor laser technique

In addition to the above techniques, another photonic generation technique for UWB signals is to excite the relaxation oscillations of a semiconductor laser. For a semiconductor laser, when it is modulated by a direct driving current or an external injected optical modulation signal, relaxation oscillation plays an important role on the dynamic response. Moreover, due to the existence of relaxation oscillation, the shape of the output of the semiconductor laser differs from that of the input signal [84]. Recently, photonic generation of UWB signals techniques based on direct modulation of a semiconductor laser [84, 85] or cross gain modulation (XGM) of a semiconductor laser externally injected by a modulated optical signal [86-91] have been proposed and experimentally demonstrated.

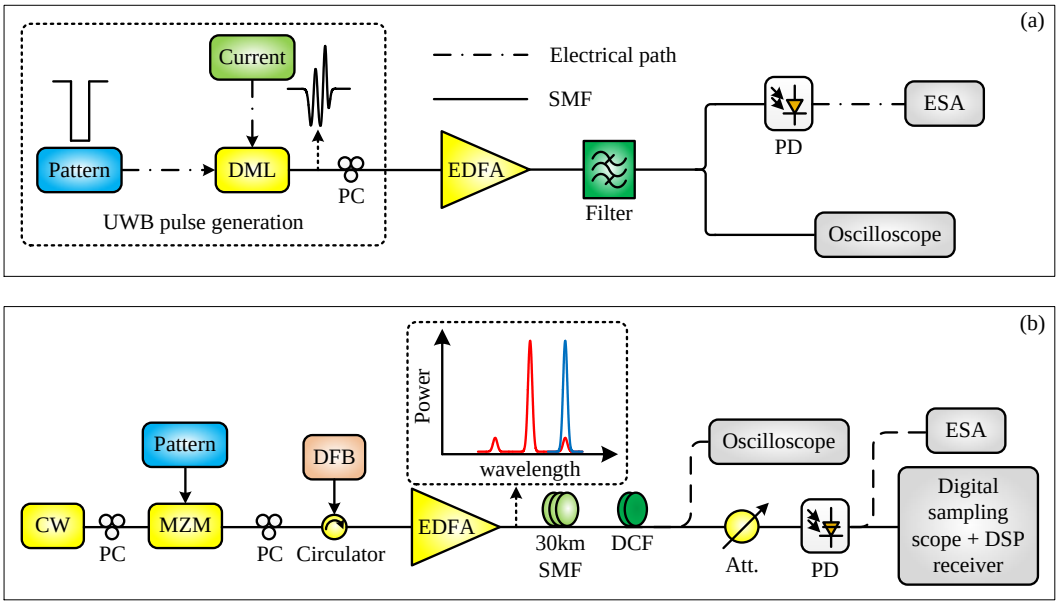

Fig. 2.6. Schematic diagram of the photonic UWB generation technique based on the relaxation oscillations of (a) a direct modulation laser (DML) and (b) an optically injected DFB laser [84]. MZM: Mach-Zehnder modulator; DCF: dispersion compensation fiber; Att.: attenuator; ESA: electrical spectrum analyzer; DSP: digital signal processing.

Fig. 2.6(a) shows the schematic diagram of the photonic UWB generation technique based on the relaxation oscillations of a DML. The architecture for the generation part is quite simple which only consists of a DML and a pulse pattern generator. The electrical modulation signal is a pattern sequence with a form of "0101 1111 1111 1111". The principle of the scheme is that the carrier density in the active region of the DML changes with the modulation current, which leads to the change of the photon density as well. In the output waveforms, two intensive

overshooting peaks and some subsequent weak vibrations appear due to the relaxation oscillation, and double-valley shapes appears due to the double zeros in the electrical driving pattern. The accumulated effect of the electrical driving current and the relaxation oscillation leads to the generated pulse shape close to that of UWB pulses with higher order [84]. After the photodetection at the PD, the desired electrical UWB impulses are generated.

Fig. 2.6(b) shows the schematic diagram of the photonic UWB generation technique based on the relaxation oscillations of an optically injected DFB laser. A CW light is intensity-modulated by an electrical pulse pattern at an MZM. The electrical pulse pattern is a 32-bit high speed sequence of the form “1010 0000 0000 0000” and “0101 1111 1111 1111”. The intensity-modulated optical signal at the output of the MZM is then injected into a DFB laser. The DFB laser here is biased above laser threshold for digital zero level. Due to the relaxation oscillations, a transient overshoot beyond the steady state takes place for input bit 1 and an undershoot for an input bit 0 [89]. Therefore, similar to the condition in [84], in the output waveform, there also exist intensive overshooting peaks and some subsequent weak vibrations. At the DFB laser, the emitting wavelength is cross-gain modulated by the injected optical signal. The wavelength of the CW light is chosen to be located at the first-order sideband of the DFB laser to

enhance the XGM between the injected light and the DFB emitting wavelength [89], as can been seen from Fig. 2.6(a). Due to the XGM, the DFB emitting optical signal is of a π phase shift with reshaped waveforms relative to the injected signal. Then the output signals are amplified and transmitted through a length of SMF and DCF. After optical to electrical conversion at a PD, the optical signals at the two wavelengths are combined. Since the two signals are out of phase, the combination of the original 0 and 1 part of the waveforms results in a constant power level and the only left time-varied waveforms are from the injection induced relaxation oscillation at the DFB laser. This process is the incoherent summation of the optical field of the two optical signals. The generated signal is a sequence of UWB impulses with binary phase. The original driving pattern form "1010 0000 0000 0000" and "0101 1111 1111 1111" corresponds to the UWB pulses with 0 and π phase shift respectively. Due to the double ones and zeros in the pattern, the generated UWB impulses are also with higher order [84].

In both schemes, the generated UWB impulses are of higher orders than that of a Gaussian monocycle or doublet. This character enables better exploitation of the assigned UWB frequency band.

2.2.2 Wavelength reuse in a UWB over WDM-PON

In a WDM-PON, wavelength reuse has been proposed as an effective solution to realize a "colorless" ONU where the upstream service shares the same wavelength channel as that of the downstream service [29, 42-45]. In such a network, colorless ONUs are equally equipped with low-cost and stable receivers for downstream signals and transmitters for upstream signals. Therefore, simple structure and the ability to enable the system to realize bidirectional transmission with a centralized light source at the OLT is the design principle of a colorless ONU. In addition, the impact on the upstream transmission from the downstream signal has to be minimized. Aiming at these requirements, numerous solutions have been proposed and demonstrated. In general, wavelength reuse can be realized through three major approaches. First, injection locking of an FP-LD; second, gain-saturation of an RSOA; third, utilization of a separated optical carrier for uplink connection. In this section, an introduction about these wavelength reuse techniques is presented.

2.2.2.1 Injection locking of an FP-LD technique

For an injection locked FP-LD based wavelength reuse scheme, an FP-LD is placed at each ONU to be injection locked by the downstream optical signal and

acts as an optical carrier generator for the uplink. When the FP-LD is injection locked, it will lase at the same wavelength as the injected downstream signal with the original data largely suppressed, thus enables the output wavelength to be used for upstream data transmission [25].

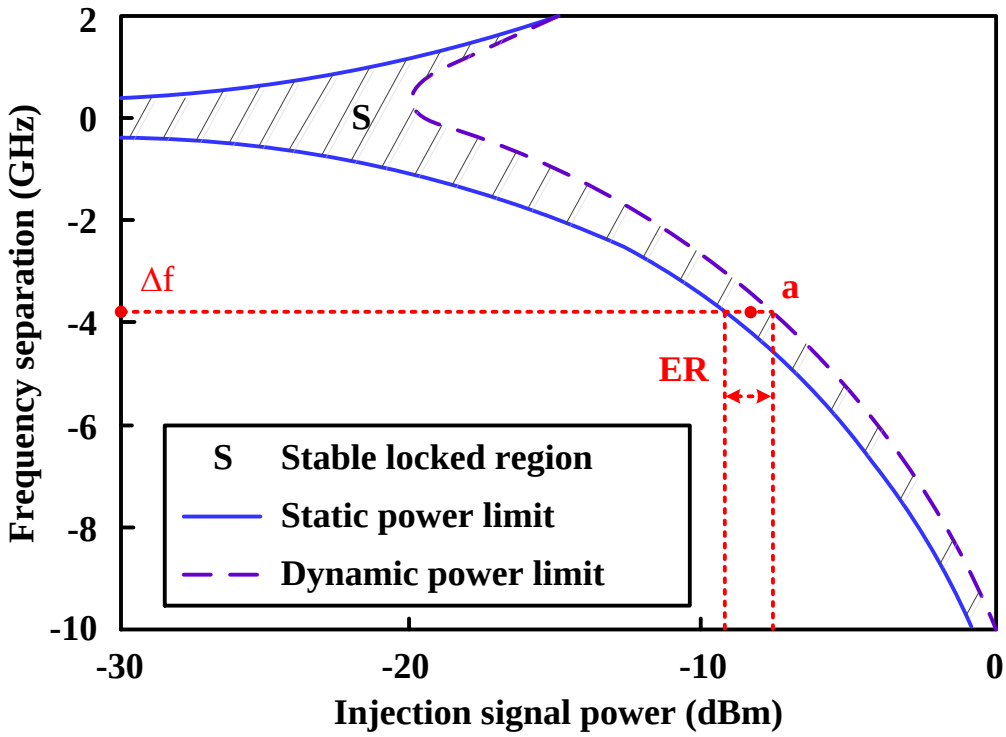

Fig. 2.7. Injection locking property of a semiconductor laser [92]. The output optical power of the semiconductor laser is assumed to be 0 dBm.

For a semiconductor laser with a given output power, injection locking of the laser is determined by the injection power and the frequency separation, $\Delta f = f_s - f_i$, where f_s is injection wavelength and f_i is the free running wavelength. Fig.

2.7 shows the relationship between the injection power and the frequency separation [92]. To ensure stable injection locking, the injection power must be confined in a region determined by the smallest injection power required to ensure effective injection locking (static power limit) and the maximum injection power limited due to the relaxation oscillation (dynamic power limit) [92]. A strong injection power may lead to relaxation oscillation, thus the injection power should not be too large. The static and dynamic power limits can be obtained through finding the stationary solutions of the rate equations of the injection locking system [93, 94]. The solid line gives the region defined by the static power limit. The dashed line defines the border of relaxation oscillation. Stable operation is ensured if the injection power and the injection wavelength are within the shadowed region. In this stable locking region, the output optical power from the FP-LD is constant with the original data on the injected signal largely suppressed, meanwhile, the FP-LD lases with the same wavelength as the injected signal. Therefore, by properly controlling the injected wavelength and power, a clear optical carrier can be generated. However, it should be noted that the ER of the injected signal must be controlled below the limitation set in Fig. 2.7, this in turn limits the modulation depth of the downstream signals. In addition, a negative frequency detuning is observed from Fig. 2.7, which means the locking wavelength is shifted toward a longer wavelength when the injected power

increases. This is due to the dependence of the refractive index on the carrier density in the cavity active region [95]. Based on the above principle, various injection locking schemes have been proposed [46-49].

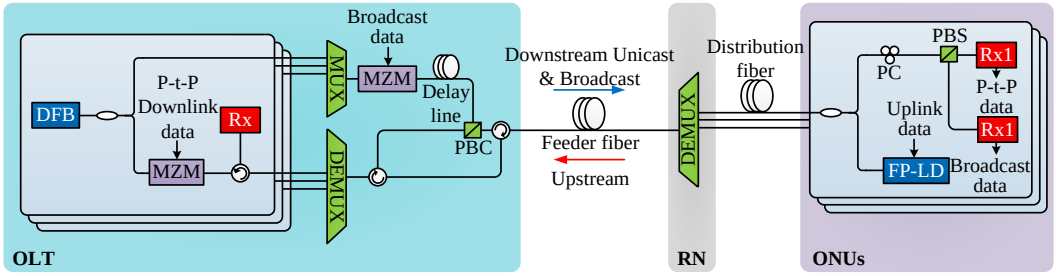

Fig. 2.8. Architecture of a broadcast-capable WDM-PON based on polarization-sensitive weak-resonant-cavity FP-LD [48]. P-t-P: point-to-point; Rx: receiver; MUX: multiplexer; DEMUX: de-multiplexer; PBC: polarization beam coupler; RN: remote node; PBS: polarization beam splitter.

Fig. 2.8 shows the system architecture of a wavelength reuse scheme based on an injection locked FP-LD. At the OLT, the optical carrier from each DFB laser is first split into two portions. One portion is first modulated by the downstream P-t-P unicast data and then wavelength multiplexed. The other portion is first wavelength multiplexed and then modulated by the broadcast data simultaneously. The delay line at one branch is used to de-correlate the phase of the two branches from the same wavelength. Then the unicast signals and the broadcast signal are polarization multiplexed at a PBC and transmitted to the RN through the feeder

fiber where they are wavelength de-multiplexed by a DEMUX and distributed to the corresponding ONU. At each ONU, the downstream signal is divided into two parts. One part of sent to a PBS, which is used to polarization de-multiplex the downstream unicast and broadcast signals. Then the de-multiplexed signals are detected by the corresponding receiver. The other part is applied to an FP-LD to injection lock one of its longitudinal modes. The FP-LD used here is directly modulated by the uplink data. Therefore, the output of the FP-LD is the uplink intensity-modulated signal with the original downstream data largely suppressed. The uplink signals are then multiplexed and transmitted through the same feeder fiber back to the OLT where they are de-multiplexed and detected respectively.

The FP-LD based wavelength reuse technique is enabled to contribute to simple ONUs, as can be seen from the above example. However, just as discussed before, the uplink transmission is sensitive to the ER of the downstream signals. When the ER of the downstream signals increases, the performance of the uplink transmission is severely degraded. Therefore, the ERs of the downstream signals have to be precisely controlled to balance the tradeoff between downstream and upstream performance. In the illustrated experiment, such experimental phenomenon is clearly observed [48].

In this thesis, a new FP-LD based wavelength reuse scheme is proposed and experimentally demonstrated where such limitation on the downstream ER is greatly reduced. The detailed presentation of this work will be shown in Chapter 4.

2.2.2.2 Gain-saturation of an RSOA technique

RSOA based wavelength reuse technique has been considered to be a very attractive solution to realize a simple and cost effective ONU due to the competitive character. First, RSOA based wavelength reuse technique can realize fully colorless ONUs, where the only mattered factors are the ER and the power of the input optical signal. Second, relatively low input saturation power contributes to a better power budget. Although saturated SOA based data rewriting scheme is also colorless [96], costly extra preamplifier is need, which may greatly increase the expense of each ONU [50]. In addition, the ability of direct modulation eliminates the necessity of an external modulator, which further reduce the system cost.

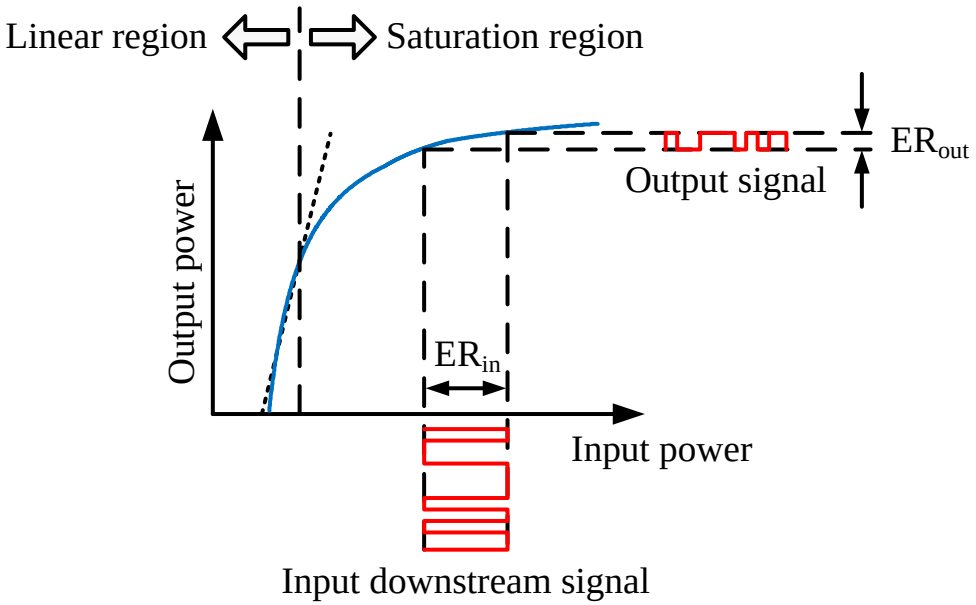

Fig. 2.9. Transfer function and data erasing principle of the RSOA used in a wavelength reuse scheme [96, 97].

Fig. 2.9 shows the transfer function and data erasing principle of the RSOA in a wavelength reuse scheme. The blue line in the figure is the transfer function of the RSOA. The linear region and saturation is divided by a dashed line. To realize the data erasing, the input downstream is supposed to be set within the saturation region. It can be clearly seen in the figure that the ER of the out signal is squeezed compared with that of the input signal, i.e., $ER_{out}<ER_{in}$. If the ER of the input downstream signal is not very large, the output signal will have a constant power, which means a clear optical carrier is generated at the output of the RSOA. If the RSOA is modulated by the uplink data, then an intensity-modulated upstream signal is directly generated. However, there also exists a limitation for this

wavelength reuse technique: the ER of the input downstream signal has to be relatively low, otherwise, the remaining downstream data in the output signal will severely deteriorate the signal to noise ratio (SNR) of the upstream signal. Due to the simple and effective character of a gain-saturated ROSA for data erasing and uplink data modulation, RSOA based wavelength reuse schemes have been extensively studied [50-53].

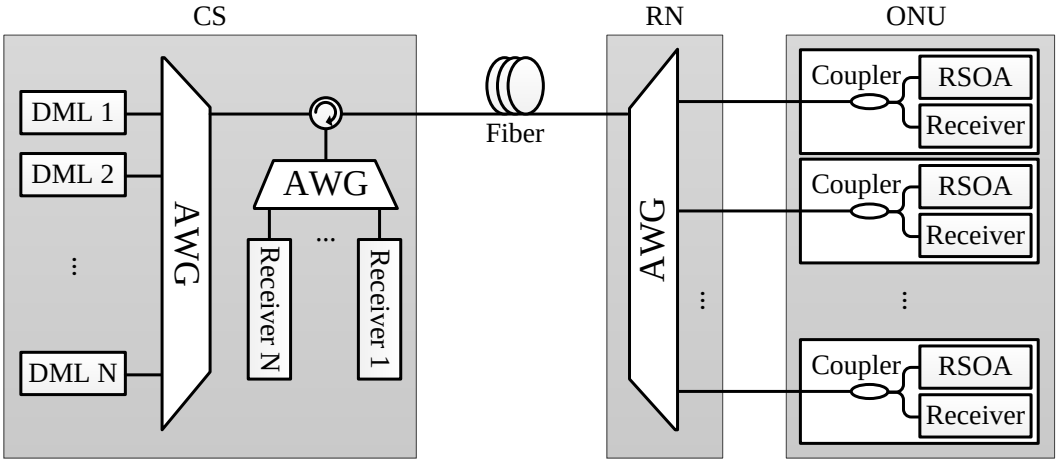

Fig. 2.10. System architecture of a wavelength reused WDM-PON based on a gain-saturated RSOA [50]. AWG: arrayed waveguide grating.

Fig. 2.10 shows the system architecture of a wavelength reused WDM-PON based on a gain-saturated RSOA. The downstream optical signals are generated by directly modulating the DML at the CS. The downstream signals are then wavelength multiplexed at an AWG and transmitted through a length of fiber to the RN where they are wavelength de-multiplexed and distributed to

corresponding ONUs. At each ONU, the downstream signal is divided into two portions by a coupler: one is received by the downstream receiver and the other is applied into an RSOA as the seeding optical signal. The downstream data is erased at the RSOA and uplink data is modulated on the downstream wavelength by directly modulating the RSOA. All the upstream optical signals are wavelength multiplexed and transmitted through the same fiber back to the CS where they are detected by corresponding receivers.

Although the system architecture of such RSOA based WDM-PON is simple, some issues regarding the RSOA need to be carefully addressed [50]. First, the average power of the input downstream signal into the RSOA should be high enough to be located within the gain-saturation region. The input saturation power is defined as the optical power injected into the RSOA where the optical gain decreases by 3 dB [50]. With higher input power, the ER of the input signal can be suppressed to a lower level and this in turn reduces the power penalty for the upstream transmission. However, the input power cannot exceed the upper limitation set by the total power budget of the link and the output power of the DML. Therefore, the input power must be controlled at a balanced value. Second, the power ratio of upstream signal to Rayleigh backscattered noise is sufficiently large [50]. This condition can be satisfied by increasing the input signal power or

tuning the RSOA gain to a higher level. Third, similar to the condition for an FP-LD, the ER of the input signal should not be too high to ensure a relatively low power penalty for the upstream signal.

2.2.2.3 Optical carrier separation technique

For a separated optical carriers based wavelength reuse technique, there exists a significant difference compared with the two previous techniques: the upstream and downstream signals occupy different frequency bands. This is because in the separated optical carrier schemes, different optical carriers for downstream and upstream transmission are employed. However, since the optical carriers for downstream and upstream transmission still derive from the same wavelength at the OLT, i.e., only one wavelength is needed for bidirectional transmission in one channel, we classify this technique as one of the wavelength reuse techniques. The most obvious advantage of this technique is that the crosstalk between the bidirectional transmissions will be insignificant since different frequency bands are assigned. This wavelength reuse technique has been widely investigated in radio over fiber system [54-57]. Recently, bidirectional transmissions in WDM-PON networks based on optical carrier separation have also been proposed and experimentally demonstrated [98, 99].

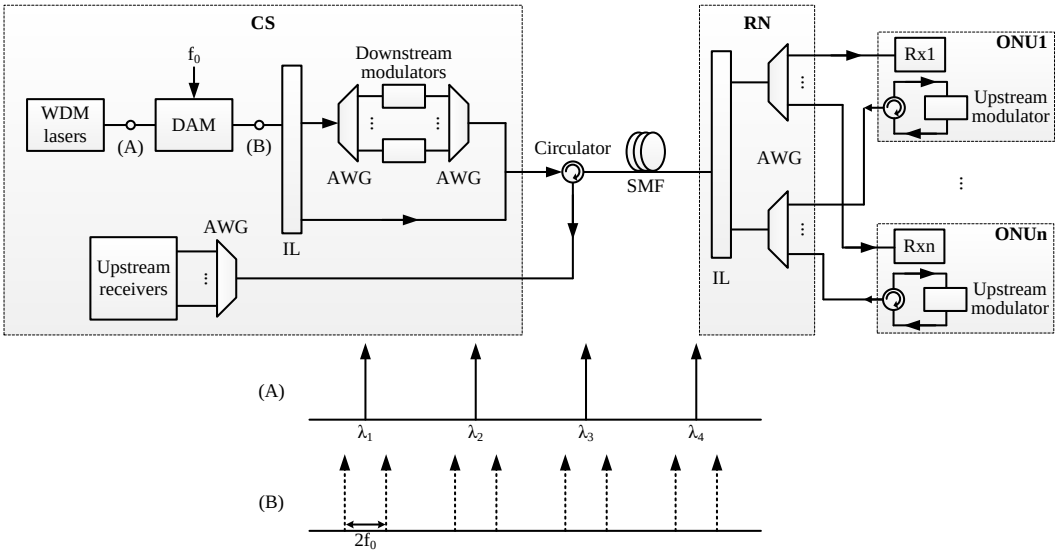

Fig. 2.11. System architecture of a wavelength reused WDM-PON based on optical carrier separation [99]. DAM: dual-arm modulator; IL: interleaver.

Fig. 2.11 shows the system architecture of a wavelength reused WDM-PON based on optical carrier separation. The light source in the system is a laser array at the CS, shown as the WDM lasers in Fig. 2.11. *N* CW lights from the WDM lasers are first applied to a DAM which is driven by an RF signal with single frequency f_0. By tuning the bias voltage of the DAM, carrier suppression can be realized [100]. Point A and B shows the input and output wavelengths of the DAM. As can be seen, *N* original optical carriers have been suppressed and *N* generated wavelength pairs is separated by $2f_0$. The wavelength pairs are then separated by an IL, where *N* odd wavelengths are used for downstream transmission and *N* even wavelengths are for upstream transmission. The *N* odd wavelengths are

wavelength de-multiplexed and modulated by corresponding downstream data and multiplexed again by a pair of AWGs. The odd and even wavelengths are then combined and transmitted through a length of SMF to the RN where they are separated by an IL. Each odd wavelength is de-multiplexed by an AWG and distributed to the corresponding ONU, where the downstream data is detected by a receiver. Correspondingly, the even wavelengths are also guided to each of their target ONUs where the wavelength is modulated by an upstream signal. The upstream signals are sent back to the OLT through the same SMF where they are routed to the corresponding upstream receivers.

In separated optical carrier based system, although the downstream and upstream transmission are based on different optical carriers, the ONUs are all colorless and only one source light at the CS is needed in each channel, i.e., bidirectional transmission is realized through centralized light source. Due to the different utilized optical carriers for the bidirectional transmission, insignificant crosstalk between the downstream and upstream signals needs to be considered.

2.3 Summary

In this chapter, the necessity of UWBoF and the integration of UWBoF into a WDM-PON were discussed, due to the intrinsic characters of UWB wireless signals and the worldwide consensus that current TDMA-PON would evolve towards WDM-PON. A conceptual illustration of UWBoF system was presented. Then, two key technologies, which were photonic generation of UWB signals and wavelength reuse, to implement UWB over WDM-PON were systematically reviewed. The major approaches to realize these two technologies were explained in detail. Meanwhile, the limitations of current wavelength reuse approaches were indicated.

Chapter 3

Bidirectional UWB-over-Fiber System Based on PM-IM Conversion and Destructive Interferencing

3.1 Introduction

In this chapter, a wavelength reuse scheme for UWBoF system based on PM-IM conversion and destructive interferencing using a PolM and an FBG is proposed and experimentally demonstrated. In the proposed system, a PolM is modulated by a Gaussian pulse train coded by a PRBS pattern to produce two opposite phase-modulated signals along the two principal axes. The phase-modulated Gaussian signal is PM-IM converted into intensity-modulated Gaussian doublet pulse train at the FBG, where the FBG is used as a frequency discriminator. The downstream signal is then sent to a BS through an optical fiber. When the principle axis of the polarizer at the BS is aligned with one of the two orthogonal polarization states, the downstream UWB signal is received and detected. On the other hand, when the principle axis of the polarizer is controlled at a special angle to one of the two orthogonal polarization states, the two projected optical signals on the principle axis of the polarizer would lead to the generation of two

complementary intensity-modulated UWB signals and cancel each other, then a clear optical carrier without intensity modulation is generated at the output of the polarizer, and it is reused for upstream UWB data transmission.

The proposed wavelength reuse scheme for a UWBoF system has the following advantages. First, a clear optical carrier without intensity modulation for upstream transmission can be generated at the BS, and the erasing process of the downstream data is independent of the modulation depth and data rate of the downstream signal. For the schemes using separated optical carriers, part of the carriers are not modulated but intended for upstream modulation, the modulation efficiency is thus relatively low. In addition, the demodulation of the subcarrier multiplexed downstream signal at the BS is complicated and costly. It also should be noted that, when broader signal bandwidth is required, the channel spacing of WDM-PON has to be increased to ensure nonoverlapping assigned frequency bands for bidirectional transmission. In the proposed scheme, the UWB signal is directly generated and modulated on the optical carrier in the optical domain at the CS. At the BS, the upstream service shares exactly the same carrier as the downstream one, which means the optical carrier is completely used for both downstream and upstream services. For the schemes using FP-LDs and RSOAs, there is a tradeoff between the ERs of the downstream and upstream signals, while

in the proposed scheme the modulation depth of the downstream signal has negligible impact on the performance of the upstream service. Second, the wavelength reuse at the BS of the proposed system is based on adjusting the principle axis of the polarizer, no active element is utilized. Therefore, there are no additional noise and nonlinearity imposed on the generated optical carrier. This property also contributes to a much clearer optical carrier for upstream transmission.

A detailed theoretical analysis of the UWB signal generation and detection and wavelength reuse process is presented. A bidirectional point-to-point transmission of 1.25 Gb/s UWB signal over 25-km SMF is experimentally demonstrated. The performance including the eye diagrams, the BERs and the power budget is evaluated. An error free transmission of both signals over a 25-km SMF is achieved. A power penalty due to the wavelength reuse is measured to be as low as 0.2 dB.

3.2 Design of the UWB-over-fiber system

In this section, a detailed description of the proposed UWBoF system is given. The system architecture is explained and illustrated. A theoretical model for UWB signal generation and detection as well as the wavelength reuse process is developed.

3.2.1 System architecture

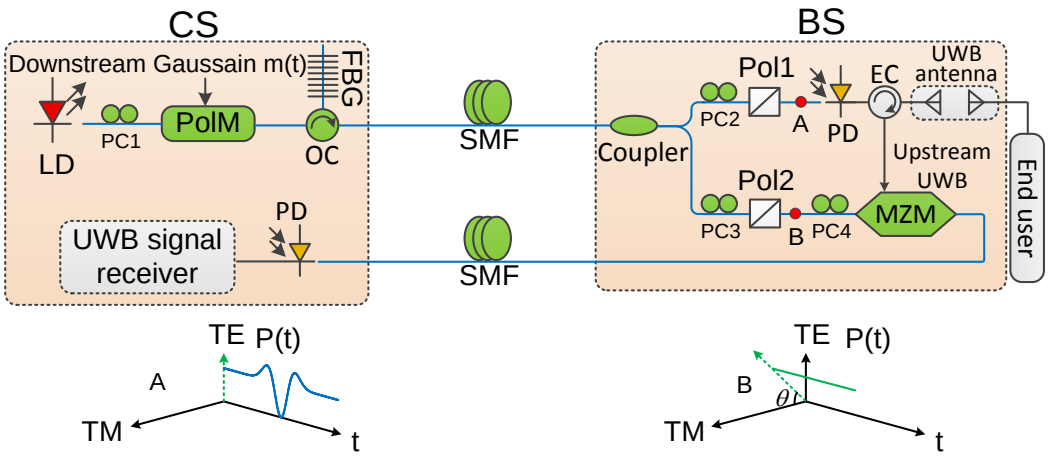

Fig. 3.1. The proposed UWBoF architecture with wavelength reuse based on a PolM and an FBG. DS: downstream; US: upstream; EC: electrical circulator; TE: transverse electric; TM: transverse magnetic.

The schematic of a UWBoF system incorporating our proposed new wavelength reuse scheme is shown in Fig. 3.1. At the CS, the transceiver consists of an LD, a

PC, a PolM, an FBG, a PD, and a UWB signal receiver. A linearly polarized CW light wave emitted from the LD is sent to the PolM through PC1. The PolM is a special phase modulator that supports phase modulations along the two principle axes but with opposite modulation indices. The incident light wave is orientated at an angle of 45 ° relative to one principle axis of the PolM. Thus, the light wave is projected to the two principle axes with an identical optical power. The PolM is driven by a Gaussian pulse train coded in a PRBS pattern via the RF port. Two phase-modulated signals from the PolM are thus generated and sent to the FBG via an optical circulator (OC). When the wavelength of the light wave is located at the linear slope or quadrature slope of the FBG spectral response, the FBG operates as a frequency discriminator to perform PM-IM conversion. Downstream optical signal from the CS is sent to the BS through a length of SMF.

At the BS, the received optical signal is divided into two portions. Each portion is sent to a polarizer through a PC (PC2, PC3). By adjusting the principle axis of the polarizer to align with one of the two orthogonal SOPs of the incoming optical signal, the downstream optical signal can be received. To erase the downstream data, the principle axis of the polarizer should be tuned to a special angle to one of the two orthogonal SOPs, then the carrier can be reused for upstream transmission. As shown in Fig. 3.1, the upper portion is for the downstream signal

transmission. The principle axis of the polarizer (Pol1) is aligned to one of the two orthogonal SOPs of the incoming signal. At the output of Pol1, only the aligned polarization mode is selected while the orthogonally polarized mode is completely attenuated. Then, the optical signal is sent to a PD and the detected electrical UWB signal is radiated to free space via a UWB antenna. A detailed theoretical analysis of the UWB signal generation and detection will be presented in Chapter 3.2.2. The lower portion of the optical signal is used for wavelength reuse. As shown in Fig. 3.1, the principle axis of the polarizer (Pol2) is controlled at a special angle to one of the two orthogonal SOPs of the incoming optical signal. At the output of Pol2, a clear optical carrier without intensity modulation is obtained and is used for upstream transmission. In Chapter 3.2.3, a detailed theoretical analysis of the data erasing process will be presented. Then, the generated optical carrier is modulated by an upstream UWB signal at a Mach-Zehnder modulator (MZM) and is used for upstream UWB signal transmission. The upstream signal from the BS is sent back to the CS through a length of SMF. At the CS, the optical signal is sent to a PD and then demodulated by a UWB signal receiver.

3.2.2 UWB signal generation and detection

At the CS, the key component of the transceiver is the PolM, which is a special PM that supports both TE and TM modes with opposite phase modulation indices

[2]. When the SOP of the linearly polarized CW light is oriented at an angle of 45° relative to one principle axis of the PolM, two complementary phase-modulated signals are generated along the two principal axes [2]. The normalized optical field of the two complementary phase-modulated signals along the two principle axes at the output can be expressed as

$$E_1(t)=\begin{bmatrix}E_{x1}(t)\\E_{y1}(t)\end{bmatrix}=e^{j\omega_c t}\begin{bmatrix}e^{j\beta m(t)/2}\\e^{-j\beta m(t)/2}\end{bmatrix}, \tag{3-1}$$

where ω_c is the angular frequency of the optical carrier, β is the phase modulation index of the PolM, and $m(t)$ is the modulation signal, which is a Gaussian pulse train coded in a PRBS pattern.

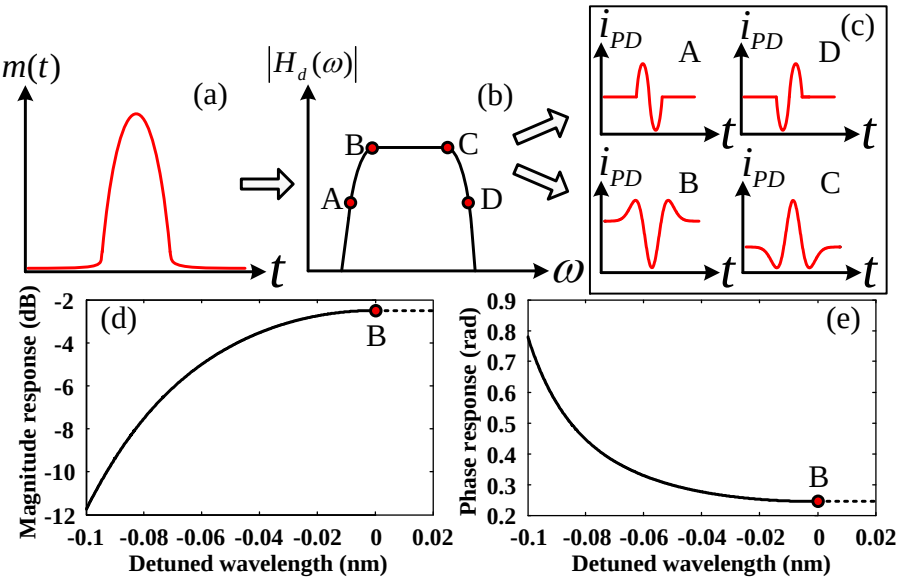

Fig. 3.2. Reflection spectrum of the FBG-based frequency discriminator and UWB pulse generation based on PM-IM conversion. (a) Temporal waveform of

the Gaussian pulse; (b) magnitude reflection spectrum of the FBG-based frequency discriminator; (c) output waveform of the PM-IM converted signals after photodetection; (d) zoom-in view of the magnitude reflection spectrum around point B; (e) zoom-in view of the phase response of the FBG-based frequency discriminator around point B.

The two phase-modulated signals are then sent to the FBG via the OC. When the optical carrier is located at a linear slope of the FBG reflection spectrum, as shown at point **A** or **D** in Fig. 3.2, the FBG is operating as a linear frequency discriminator where the phase-modulated signal is converted to an intensity-modulated signal. Mathematically, PM-IM conversion in a linear frequency discriminator corresponds to a first-order differentiator [101]. If the modulation signal is a Gaussian pulse, the output signal is a Gaussian monocycle. On the other hand, when the optical carrier is located at a quadrature slope of the FBG reflection spectrum, as shown at point **B** or **C** in Fig. 3.2, the FBG also serves as a frequency discriminator, but with a quadratic frequency response, given by

$$H_d(\omega) = \left[b - K(\omega - \omega_0)^2 \right] + jC \,, \tag{3-2}$$

where b, K, and C are constants, and ω_0 is the angular frequency at the maximum of $|H_d(\omega)|$. The optical carrier is set to be at point **B,** as shown in Fig. 3.2.

TABLE I

PHYSICAL REPRESENTATIONS AND VALUES OF THE PARAMETERS

Symbol	Physical representation	Value
b	parameter that determines the profile of the FBG reflection spectrum	0.7279
K	parameter that determines the profile of the FBG reflection spectrum	8.8570×10^{-23} (s/rad)
$\lvert\omega_c-\omega_0\rvert$	frequency detuning of the optical carrier with respect to the peak of the parabola	0 (rad/s)
C	parameter that determines the profile of the FBG reflection spectrum	0.1820
β	phase modulation index of the PolM	0.5928 (rad/V)
$m(t)$	modulation signal: PRBS Gaussian pulse train	1.8 (V) (peak-to-peak amplitude)
$m'(t)$	first-order derivative of the modulation signal	4.3664×10^{10} (V) (peak-to-peak amplitude)
$m''(t)$	second-order derivative of the modulation signal	1.0412×10^{21} (V) (peak-to-peak amplitude)

The values of the parameters mentioned in (3-2) are given in Table I. By applying the values of all the parameters in (3-2), the frequency responses in magnitude and

phase of the FBG based on this theoretical model are plotted at Fig. 3.2(d) and (e). Then, the signal at the output of the FBG in the frequency domain is given by

$$E_2(\omega)=\begin{bmatrix}E_{x2}(\omega)\\E_{y2}(\omega)\end{bmatrix}=\left[b-K(\omega-\omega_0)^2+jC\right]\begin{bmatrix}E_{x1}(\omega)\\E_{y1}(\omega)\end{bmatrix}, \tag{3-3}$$

where $E_{x1}(\omega)$ and $E_{y1}(\omega)$ are the Fourier transforms of $E_{x1}(t)$ and $E_{y1}(t)$, respectively. $E_{x2}(\omega)$ and $E_{y2}(\omega)$ are the Fourier transforms of the signals at the output of the FBG along the two orthogonal SOPs.

Applying the inverse Fourier transform to (3-3), the signal in the time domain is given by

$$\begin{aligned}
&E_2(t)=\begin{bmatrix}E_{x2}(t)\\E_{y2}(t)\end{bmatrix}\\
&=F^{-1}\left\{\left[b-K(\omega-\omega_0)^2+jC\right]E_1(\omega)\right\}\\
&=F^{-1}\begin{Bmatrix}bE_1(\omega)-K\omega^2E_1(\omega)+2K\omega_0\omega E_1(\omega)\\-K\omega_0{}^2E_1(\omega)+jCE_1(\omega)\end{Bmatrix}\\
&=bE_1(t)+KE_1''(t)+\frac{2K\omega_0}{j}E_1'(t)-K\omega_0{}^2E_1(t)+jCE_1(t)\\
&=\begin{Bmatrix}b-K\left[\omega_c-\omega_0+\beta m'(t)/2\right]^2+jK\beta m''(t)/2+jC\\b-K\left[\omega_c-\omega_0-\beta m'(t)/2\right]^2-jK\beta m''(t)/2+jC\end{Bmatrix}\begin{bmatrix}E_{x1}(t)\\E_{y1}(t)\end{bmatrix}
\end{aligned}, \tag{3-4}$$

where $E_{x2}(t)$ and $E_{y2}(t)$ are the two PM-IM converted signals along the two orthogonal SOPs; $m'(t)$ and $m''(t)$ are the first and second order derivatives of the modulation signal, respectively.

In (3-4), the angular frequency of the optical carrier ω_c is set to be identical to ω_0, i.e., the input optical carrier is located at the peak point of the parabola in this model. Then, (3-4) can be rewritten as

$$\begin{aligned} E_2(t) &= \begin{bmatrix} E_{x2}(t) \\ E_{y2}(t) \end{bmatrix} \\ &= \begin{bmatrix} b - K\left(\beta m'(t)/2\right)^2 + jK\beta m''(t)/2 + jC \\ b - K\left(\beta m'(t)/2\right)^2 - jK\beta m''(t)/2 + jC \end{bmatrix} \begin{bmatrix} E_{x1}(t) \\ E_{y1}(t) \end{bmatrix}. \end{aligned} \tag{3-5}$$

At the output of port 3 of the OC, the downstream optical signals are generated along the two orthogonal SOPs, as shown in Fig. 3.1. The optical downstream signals from the CS are transmitted to the BS through a length of SMF.

At the BS, the received optical signal is divided into two portions. Each portion is sent to a PC and a polarizer. As shown at point A in Fig. 3.1, the upper portion is for the downstream signal detection. The dotted green line in the subset marks the principle axis of Pol1, which is aligned with one SOP of the incoming signal $E_{y2}(t)$. The signal $E_3(t)$ at the output of the polarizer is expressed as

$$E_3(t) = E_{y2}(t)e^{j\varphi_y}, \tag{3-6}$$

where φ_y is an additional phase shift introduced to $E_{y2}(t)$ by PC2.

By applying the signal to the PD, a photocurrent is generated which is given by

$$\begin{aligned}
i_{PD} &= R\left|E_3(t)\right|^2 = R\left|E_{y2}(t)\right|^2 \\
&= R\left|\left\{\left[b - K\left(\beta m'(t)/2\right)^2\right] + j\left[C - K\beta m''(t)/2\right]\right\}E_{x1}(t)\right|^2 \\
&= R\left\{\left|\left[b - K\left(\beta m'(t)/2\right)^2\right] + j\left[C - K\beta m''(t)/2\right]\right|\left|E_{x1}(t)\right|\right\}^2 \\
&= R\left|\left[b - K\left(\beta m'(t)/2\right)^2\right] + j\left[C - K\beta m''(t)/2\right]\right|^2 \\
&= R\left\{\left[b - K\left(\beta m'(t)/2\right)^2\right]^2 + \left[C - K\beta m''(t)/2\right]^2\right\} \\
&= R\left\{\begin{array}{l}\left(b^2 + C^2\right) - \left[bK\beta^2\left(m'(t)\right)^2/2 + CK\beta m''(t)\right] + \\ \left[K^2\beta^4\left(m'(t)\right)^4/16 + K^2\beta^2\left(m''(t)\right)^2/4\right]\end{array}\right\}
\end{aligned}, \tag{3-7}$$

where R is the responsivity of the PD.

The first and the second terms on the right-hand side in (3-7) are dc terms. Based on the given values in Table I, the quantitative relationship between the four time-varied terms in (3-7) is calculated:

$$\left|\frac{bK\beta^2\left(m'(t)\right)^2/2+CK\beta m''(t)}{K^2\beta^4\left(m'(t)\right)^4/16+K^2\beta^2\left(m''(t)\right)^2/4}\right|>>1, \tag{3-8}$$

from which the last two terms in (3-7) can be ignored. Then, the ac term of the photocurrent is:

$$i_{ac}=-\mathrm{R}\left[bK\beta^2\left(m'(t)\right)^2/2+CK\beta m''(t)\right]. \tag{3-9}$$

The detected signal after the PD is related to the first- and the second-order derivatives of the modulation signal. A simulation is performed to show the shape of the detected downstream pulse. Since the modulation signal is a Gaussian pulse train, addition of the two terms in (3-9) leads to a Gaussian doublet shaped pulse, as shown by the simulated waveform in Fig. 3.3. Therefore, the received electrical UWB signal is a Gaussian doublet pulse train [6].

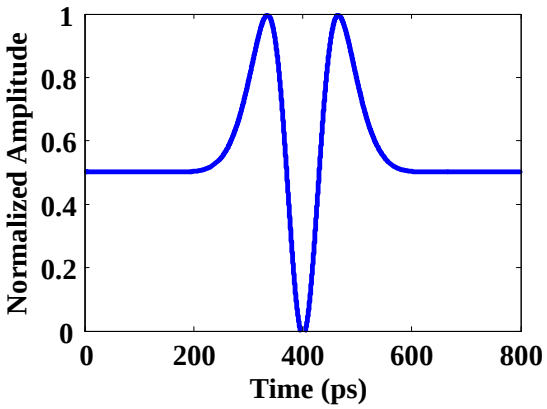

Fig. 3.3. Detected downstream Gaussian doublet based on PM-IM conversion at the FBG.

At the output of the PD, the electrical UWB signal is then radiated to the end users via a UWB antenna. As a result, the link for the downstream UWB service is implemented.

3.2.3 Wavelength reuse for upstream transmission

When one of the two orthogonal SOPs of the incoming optical signal, say the TM mode, is oriented at an angle of γ to the principle axis of Pol2, as shown at point B in Fig. 3.1, then the signal at the output of Pol2 is given by

$$
\begin{aligned}
&E_3(t) = E_{x2}(t)e^{j\theta_x}\cos(\gamma) + E_{y2}(t)e^{j\theta_y}\sin(\gamma) \\
&= \left\{\left[b - K\left(\beta m'(t)/2\right)^2\right] + j\left[C + K\beta m''(t)/2\right]\right\}E_{x1}(t)e^{j\theta_x}\cos(\gamma) + \\
&\quad \left\{\left[b - K\left(\beta m'(t)/2\right)^2\right] + j\left[C - K\beta m''(t)/2\right]\right\}E_{y1}(t)e^{j\theta_y}\sin(\gamma) \\
&= \left[b - K\left(\beta m'(t)/2\right)^2\right]\left\{E_{x1}(t)e^{j\theta_x}\cos(\gamma) + E_{y1}(t)e^{j\theta_y}\sin(\gamma)\right\} + \\
&\quad \left[C + K\beta m''(t)/2\right]E_{x1}(t)e^{j(\theta_x+\pi/2)}\cos(\gamma) + \\
&\quad \left[C - K\beta m''(t)/2\right]E_{y1}(t)e^{j(\theta_y+\pi/2)}\sin(\gamma) \\
&= \left[b - K\left(\beta m'(t)/2\right)^2\right]\left\{\begin{matrix} e^{j(\omega_c t+\beta m(t)/2+\theta_x)}\cos(\gamma) + \\ e^{j(\omega_c t-\beta m(t)/2+\theta_y)}\sin(\gamma) \end{matrix}\right\} + \\
&\quad \left[C + K\beta m''(t)/2\right]e^{j(\omega_c t+\beta m(t)/2+\theta_x+\pi/2)}\cos(\gamma) + \\
&\quad \left[C - K\beta m''(t)/2\right]e^{j(\omega_c t-\beta m(t)/2+\theta_y+\pi/2)}\sin(\gamma) \\
&= \left[b - K\left(\beta m'(t)/2\right)^2\right]e^{j(\omega_c t+\theta_y)}\left[\begin{matrix} e^{j(\beta m(t)/2+\theta_x-\theta_y)}\cos(\gamma) + \\ e^{-j\beta m(t)/2}\sin(\gamma) \end{matrix}\right] + \\
&\quad e^{j(\omega_c t+\theta_y+\pi/2)}\left\{\begin{matrix} \left[C + K\beta m''(t)/2\right]e^{j(\beta m(t)/2+\theta_x-\theta_y)}\cos(\gamma) + \\ \left[C - K\beta m''(t)/2\right]e^{-j\beta m(t)/2}\sin(\gamma) \end{matrix}\right\}
\end{aligned}
\quad , \qquad (3\text{-}10)
$$

where θ_x and θ_y are the additional phase shifts to $E_{x2}(t)$ and $E_{y2}(t)$ introduced by PC3, respectively, and θ_x-θ_y is the phase shift difference between the TE and TM modes.

To obtain a clear optical carrier without any intensity modulation for the reuse for upstream transmission, the magnitude of $E_3(t)$ must be a constant, which means

$$\left|E_3(t)\right| = \sqrt{E_3(t)\cdot\left[E_3(t)\right]^*} = D, \tag{3-11}$$

where D is a constant.

Substitute (3-10) into (3-11), after some mathematical manipulations, we have the following expression for the square of the magnitude of $E_3(t)$

$$\begin{aligned}\left|E_3(t)\right|^2 &= E_3(t)\cdot\left[E_3(t)\right]^* \\ &= T_1^2 + CK\beta m''(t)\cos(2\gamma) + T_1^2\sin(2\gamma)\cos\alpha(t) - \\ &\quad T_1\sin(2\gamma)\sin\alpha(t)K\beta m''(t) + C^2\sin(2\gamma)\cos\alpha(t) + C^2 + \\ &\quad K^2\beta^2\left(m''(t)\right)^2/4 - K^2\beta^2\left(m''(t)\right)^2/4\cdot\sin(2\gamma)\cos\alpha(t)\end{aligned}, \tag{3-12}$$

where

$$
\begin{aligned}
T_1 &= b - K\left(\beta m'(t)/2\right)^2 \\
T_2 &= C + K\beta m''(t)/2 \\
T_3 &= C - K\beta m''(t)/2 \\
\alpha(t) &= \beta m(t) + \theta_x - \theta_y
\end{aligned}
\quad . \tag{3-13}
$$

In (3-12), the term $(K\beta^2 m'(t)^2/4)^2$ in T_1^2 and the term $K^2\beta^2 m''(t)^2/4$ can be neglected since they are very small compared with other terms. Thus (3-12) is rewritten as

$$
\begin{aligned}
&\left|E_3(t)\right|^2 = E_3(t)\cdot\left[E_3(t)\right]^* \\
&= \left[CK\beta m''(t)\cos(2\gamma) - bK\beta^2\left(m'(t)\right)^2/2\right] + \\
&\quad b^2\sin(2\gamma)\cos\alpha(t) - bK\beta^2\left(m'(t)\right)^2/2\cdot\sin(2\gamma)\cos\alpha(t) - \\
&\quad b\sin(2\gamma)\sin\alpha(t)K\beta m''(t) + C^2\sin(2\gamma)\cos\alpha(t) + \\
&\quad \sin(2\gamma)\sin\alpha(t)K^2\beta^3 m''(t)\left(m'(t)\right)^2/4 + C^2
\end{aligned}
\quad . \tag{3-14}
$$

By tuning PC3, θ_x-θ_y and γ can be adjusted, which controls the bias point on the cosine transfer function $\cos[\alpha(t)]$ and the value of $\cos(2\gamma)$ and $\sin(2\gamma)$.

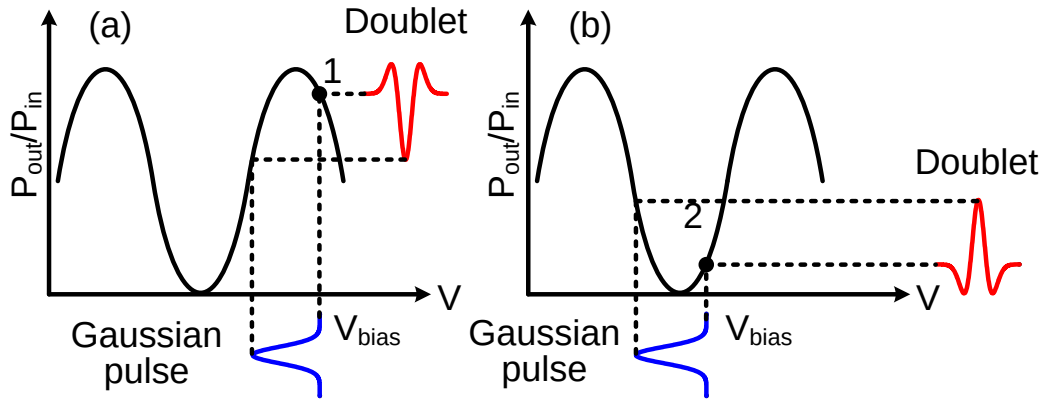

Fig. 3.4. Principle of UWB doublet generation based on the nonlinear shaping of a Gaussian pulse on a cosine transfer function [102]. (a) Biased near maximum transmission point. (b) Biased near minimum transmission point.

When the Gaussian pulse is biased near the maximum or minimum transmission point, owing to the nonlinear nature of the transfer function, the shape of the Gaussian pulse is changed. If the amplitude of the Gaussian pulse is large enough, the pedestal and peak parts of the Gaussian pulse will lie in the complementary slopes of the transfer function, resulting in the generation of a Gaussian doublet [102], as shown in Fig. 3.4. In the implementation, γ and θ_x-θ_y can be controlled by adjusting PC3 to make the Gaussian pulse nonlinearly shaped into a Gaussian doublet.

In (3-14), the first two terms represent a Gaussian doublet originating from their complex combination. The last term is a dc term. Therefore, to ensure the square of the magnitude of $E_3(t)$ to be a constant, the combination of the other terms in (3-14) should be shaped into a Gaussian doublet with the same shape and amplitude as those of the first two terms, but with opposite polarity, by adjusting γ and θ_x-θ_y.

Fig. 3.5 shows the generated Gaussian doublets based on complex combination in (3-14). The doublet in blue represents the pulse from the combination of the first two terms in (3-14); while the red doublet represents that from the combination of

the rest time-varied terms. Comparing the waveforms in Fig. 3.5, it is clearly seen that the two doublets have the same pulse shape.

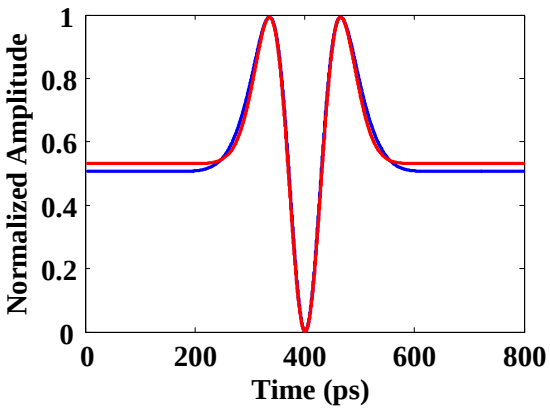

Fig. 3.5. Simulated waveforms of the generated Gaussian doublets based on complex combination.

In this calculation, the values of the parameters are given in Table I. γ and θ_x-θ_y are adjusted to be 0.5189π and 0.8550π, respectively. In addition, the peak-to-peak amplitudes of the two pulses and their difference are also obtained through the calculation, given by

$$\begin{aligned} Vpp1 &\approx Vpp2 = 0.0134 \text{ (V)} \\ Vpp1 - Vpp2 &= 3.1501\times10^{-5} \text{ (V)} \end{aligned}, \tag{3-15}$$

where $Vpp1$ and $Vpp2$ denote the peak-to-peak amplitudes of the two doublets, respectively; the peak-to-peak amplitude difference between the two pulses is

small enough. Therefore, we can conclude that two identical Gaussian doublets are generated through such complex combination of different terms. By changing the sign of γ in (3-14), the polarity of one doublet is inverted, which leads to the complete cancellation of the two pulses. In this situation, the addition of the two doublets generates a dc component, which means the output optical signal from Pol2 is a clear optical carrier with constant intensity and is suitable to be used for upstream transmission.

Note that the polarization changes during the downstream optical transmission will have impact on the performance of the system. In this condition, a polarization stabilizer at the BS is needed to compensate the polarization changes and corresponding solutions for polarization multiplexed transmission system have been proposed [103]. A polarization stabilizer should be placed at the BS right after the fiber transmission link. As can be found in [103], the polarization stabilizer is enabled to compensate the random polarization fluctuation during the fiber transmission. The two orthogonal SOPs of the downstream signal can be identified through the pilot tone. Therefore, the two orthogonal SOPs are stabilized into vertical and horizontal polarization directions [103]. The two polarizers after the polarization stabilizer can be directly adjusted at the calculated angles due to the existence of the polarization stabilizer.

3.3 Experiment

In this section, the experimental setup and the results of the conducted verification experiment is shown.

3.3.1 Experimental setup

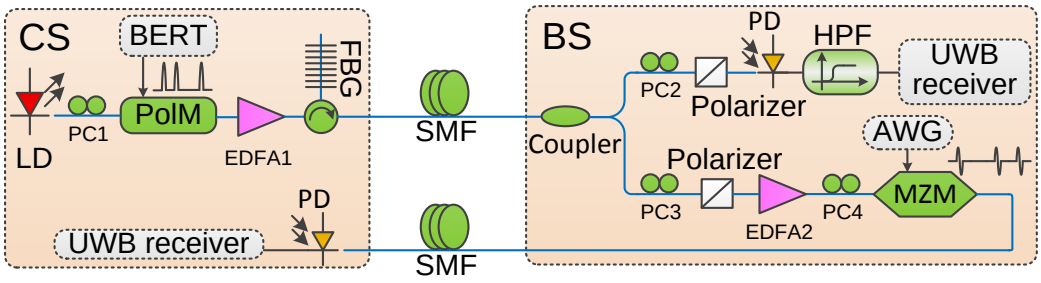

Fig. 3.6. Experimental setup of the wavelength reused UWBoF system.

The proposed wavelength reuse scheme in a UWBoF system is experimentally demonstrated. The experimental setup is shown in Fig. 3.6. At the CS, a CW light at 1555.02 nm from a tunable laser source (TLS) is applied to a PolM through PC1. The PolM (Versawave Technologies) is driven by a 1.25-Gb/s Gaussian pulse train coded in a 2^{15}-1 PRBS pattern, generated by a bit error rate tester (BERT, Agilent 4901B). The optical signal at the output of the PolM is then amplified by EDFA1 and sent to an FBG through an OC. The FBG is used as a frequency discriminator which has a center wavelength of 1556.08 nm and a

reflectivity greater than 90%. In the experiment, the wavelength of the optical carrier is controlled to be located at the left quadrature slope of the FBG reflection spectrum. Therefore, a Gaussian doublet pulse train is generated at the output of the FBG. The FBG is placed after EDFA1 to also filter out the noise induced by EDFA1. The complementary intensity-modulated downstream UWB signals are then transmitted through a 25-km SMF (Corning SM28) to the BS. At the BS, the downstream optical signal is divided into two portions by an optical coupler. In the upper portion, the downstream UWB signal is received when the principle axis of the polarizer (Pol1) is aligned with one of the two orthogonal SOPs and then sent to a 25-GHz PD. To further block the noise, a high pass filter (HPF) with a cutoff frequency of 3-GHz is utilized after the PD. Then, the electrical UWB signal is demodulated by a UWB receiver. In the lower portion, a clear optical carrier without intensity modulation is generated when the principle axis of the polarizer (Pol2) is oriented at a special angle relative to one of the two orthogonal SOPs of the incoming optical signal, as indicated in (3-14). Then, the clear optical carrier is amplified by EDFA2 and then applied to an MZM through PC4 where it is modulated by an upstream UWB signal. The upstream UWB signal is a 1.25-Gb/s UWB monocycle pulse train coded in a 2^{15}-1 PRBS pattern, generated by an arbitrary waveform generator (AWG*, Tektronix AWG 7102). The upstream optical signal is transmitted back to the CS through a 25-km SMF.

At the CS, the upstream optical signal is converted to an electrical signal at a 25-GHz PD and then sent to a UWB receiver. The performance of both downstream and upstream signal transmissions in the wavelength reused system is evaluated by measuring the eye diagrams and the bit error rates of the transmitted signals.

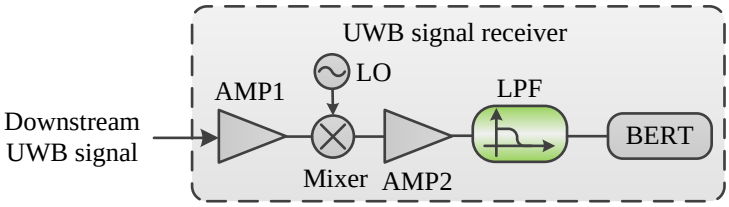

Fig. 3.7. UWB signal receiver used in the experiment.

Due to the unavailability of a UWB correlation receiver, a UWB receiver using a mixer, a structure similar to what we used in [25, 27] is utilized, as shown in Fig. 3.7. At the output of the PD, the UWB signal is first amplified by a wideband electrical amplifier (AMP1, 23-dB gain) and then applied to the mixer to mix with a local oscillator (LO) signal at 6.25 GHz. At the output of the mixer, the UWB signal is converted to a baseband signal which is amplified by a second wideband amplifier (AMP2, 10-dB gain), filtered by an LPF with a cutoff frequency of 1.2 GHz, and sent to the BERT.

3.3.2 Experimental results

At the CS, the wavelength of the CW light from the TLS is tuned to be located at the left quadrature slope of the FBG reflection spectrum. At the BS, the HPF not only blocks the noise, but also exhibits a differential effect on the input UWB signal due to the high pass characteristics. Therefore, the received electrical UWB doublet after the HPF becomes a Gaussian triplet.

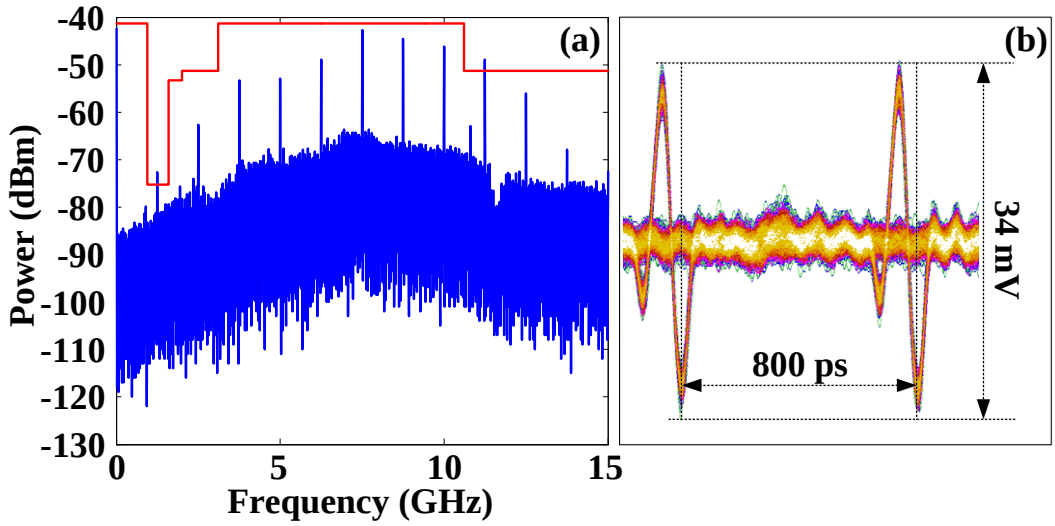

Fig. 3.8. (a) Measured electrical spectrum at 1 MHz RBW and (b) measured eye diagram of the received downstream UWB signal. RBW: resolution bandwidth.

The eye diagram as well as the electrical spectrum of the received UWB signal is measured and shown in Fig. 3.8. As can be seen, the eyes of the received downstream UWB signal are widely opened. In addition, the PSD of the UWB

signal meets the FCC spectrum mask for indoor wireless communication as well. The resolution bandwidth of the electrical spectrum analyzer is set at 1MHz when measuring the electrical spectrum of the UWB signal.

In the lower portion, by tuning the polarization direction via adjusting PC3, a clear optical carrier for upstream transmission is generated at the output of Pol2. To show the data erasing performance, we measure the temporal waveforms of the optical carrier at the output of Pol2 after photodetection when the downstream signal does not carry and carry data information.

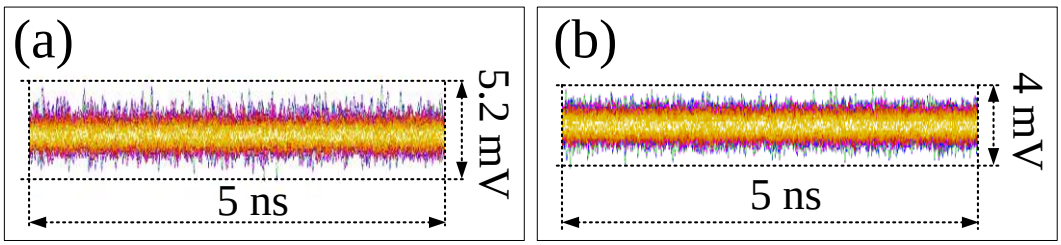

Fig. 3.9. The temporal waveform after photodetection when (a) the downstream signal does not carry data information, (b) the downstream signal carries data information, but the data is erased.

As shown in Fig. 3.9, the waveforms with or without data information are identical, indicating that the data information is completely erased. The

effectiveness of the data erasing is verified. The clear optical carrier is then used for upstream signal transmission.

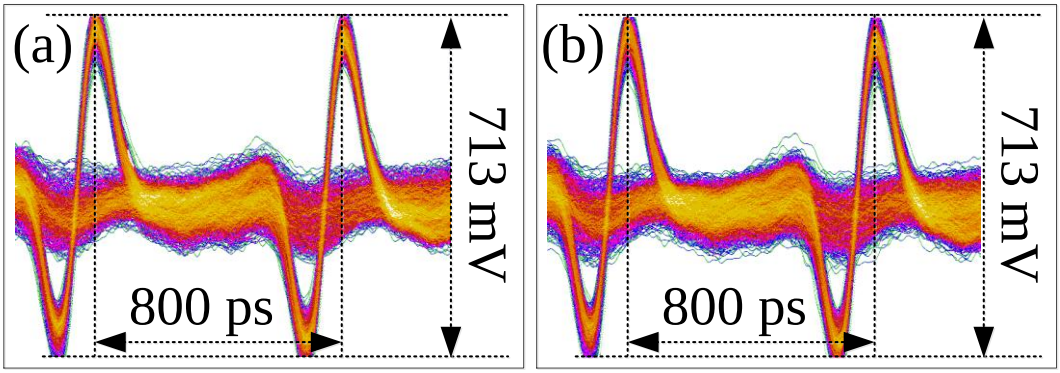

Fig. 3.10. Measured eye diagrams of the received upstream UWB signals. (a) Without a downstream UWB signal, (b) with a downstream UWB signal.

The generated optical carrier at the output of the polarizer has a power of -2 dBm and it is amplified by EDFA2. The power at the output of EDFA2 is 5 dBm. Fig. 3.10 shows the measured eye diagrams of an on-off-keying (OOK) modulated UWB upstream signal with or without a downstream UWB signal. The eyes for the two cases with or without a downstream UWB signal are both widely open, no obvious deterioration is observed for the eye diagram shown in Fig. 3.10(b). This confirms again the effective data erasing process and the good performance of the wavelength reuse scheme.

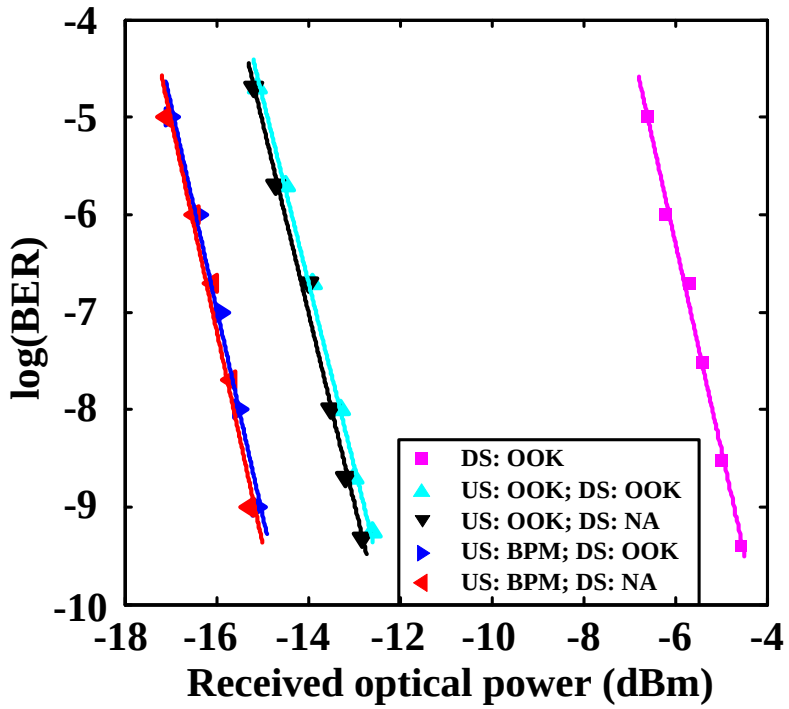

Fig. 3.11. BER measurements of the upstream UWB signals with and without a downstream signal.

Fig. 3.11 shows the BER measurements of the downstream signal and upstream signals with and without a downstream UWB signal. Error free transmission for a downstream UWB signal and an OOK or bi-phase modulation (BPM) upstream UWB signal with or without a downstream modulation is achieved. Error free transmission here is defined as the transmission of a signal in the proposed system with a BER no more than 10^{-9}. As can be observed from the BER measurements, the power penalty induced due to the existence of a downstream UWB modulation is less than 0.2 dB. In addition, the BER performance of the UWB transmission based on BPM is better than that based on OOK, providing about 2 dB additional

power margin. This is because the electrical power of a BPM modulated UWB signal is 3 dB greater than that of an OOK modulated UWB signal. The receiver sensitivities for the OOK downstream transmission, OOK and BPM upstream transmission with a downstream UWB modulation are -5 dBm, -13 dBm and -15.1 dBm, respectively. The receiver sensitivity here is defined as the optical power to obtain a BER of 10^{-9} for the UWB signal receiver. The receiver sensitivity of the downstream transmission is relatively low compared with that of the upstream transmission; this is because the effective modulation depth of the downstream UWB signal is reduced after the PM-IM conversion. The receiver sensitivity of the UWB downstream transmission can be enhanced by using an FBG with a higher reflectivity and a higher *K* value of the reflection spectrum profile. In addition, it should be noted that the receiver sensitivity of both the UWB downstream and upstream transmissions can be enhanced if a UWB correlation receiver with low noise pre-amplifiers is utilized.

The power budget of the proposed UWBoF system is evaluated and given in Table II, based on the investigation of the optical receiver sensitivities for both downstream and upstream transmissions.

TABLE II

POWER BUDGET OF THE PROPOSED UWB-OVER-FIBER SYSTEM

Downstream service		**Upstream service**	
Minimum required power at BS	**1 dBm**	**Upstream receiver sensitivity**	**-15.1 dBm**
Downstream receiver sensitivity	-5 dBm	Loss at MZM	8 dB
Loss at Pol1	3 dB	Fiber transmission and connecter loss	6 dB
Loss at coupler	3 dB	Minimum upstream optical carrier power before MZM	-1.1 dBm
Fiber transmission loss	5 dB		
Loss of other connecters	1 dB	EDFA2 output power	5 dBm
Minimum launch power from CS	**7 dBm**	**Power margin**	**6.1 dB**

In Table II, the detailed powers needed at the downstream and upstream receivers are presented. If the downstream EDFA1 is eliminated and adjust the LD output power to the maximum of 16 dBm, the output power from the CS will be 5 dBm (where the losses induced by the PolM and the FBG are 4 dB and 7 dB, respectively). The maximum attainable transmission distance is (5-1)/0.2=20 km. If the upstream EDFA2 is eliminated, after 20-km SMF transmission, the optical power after Pol2 is -2 dBm, the output power from the BS is -10 dBm, and then the maximum transmission distance for upstream service is [(-10-1)-(-15.1)]/0.2=20.5 km. The downstream and upstream transmission

distances are very close. In this experiment, since the utilized SMF has a fixed length of 25 km, therefore, optical amplification is used. In addition, the employment of the EDFAs enables the system to have a higher power margin and reduce the power requirement for the laser source at the CS.

In addition, since there is no light source in each BS, an optical amplifier is required to compensate the loss induced by the downstream and upstream link. This optical amplifier (such as an EDFA) can be placed at the remote access node and shared by multiple BSs. Moreover, the optical power required at the BS is calculated based on the measured optical receiver sensitivity in our experimental setup. We would expect that the requirement of the optical power launched into the downstream/upstream fiber link can be significantly reduced by alternatively using low-noise amplifiers at the optical receivers in both CS and BS.

3.4 Summary

In this chapter, a wavelength reuse scheme based on PM-IM conversion and destructive interferencing in a UWBoF system was proposed and experimentally demonstrated. The key contribution of the technique was the use of the PolM which was operating jointly with the FBG to generate two intensity-modulated signals along two orthogonal SOPs. The combination of the two signals at a polarizer would generate a clean optical carrier which was reused for upstream transmission. In addition, since no active elements are employed in the downstream data erasing process, no additional noise and nonlinearity are introduced, the quality of the upstream signal is thus greatly enhanced. A bidirectional point-to-point transmission of 1.25 Gb/s UWB signal over 25-km SMF was achieved. The performance including the eye diagrams, the BERs and the power budget was evaluated. An error free transmission over a 25-km SMF was demonstrated.

Chapter 4

Bidirectional UWB over WDM-PON Based on Injection Locking of an FP-LD and Polarization Multiplexing

4.1 Introduction

Of the various wavelength reuse techniques, injection locked FP-LD based scheme is considered as one major solution, as has been discussed and explained in the first two chapters. However, it should be noted that, the commonly utilized downstream injection optical signal is a baseband signal. The limitation of such an injection locking method is that the performance of the upstream signal is sensitive to the modulation depth or ER of the downstream signal. When the modulation depth of the downstream baseband signal increases, the injection-locked optical carrier at the output of the FP-LD is severely degraded, which is not suitable for upstream data re-modulation. Therefore, there is an obvious trade-off between the ER of the downstream signal and the performance of the upstream signal.

In this chapter, a wavelength reuse scheme for symmetric UWB over WDM-PON based on injection locking of an FP-LD and polarization multiplexing is proposed and experimentally demonstrated. It is different from the previous injection locking solutions where the injection signal is the downstream baseband signal; here the injection signal is a downstream UWB signal. It is demonstrated that the injection locking of an FP-LD using a UWB signal would make the upstream service performance less sensitive to the ER of the downstream UWB signal than the baseband signal, and the use of the downstream UWB signal as the injection signal would contribute to a better transmission performance for both downstream and upstream services.

In the proposed system, a PRBS UWB signal and a PRBS baseband signal are modulated on an optical carrier at two MZMs in a transceiver at the OLT, and are polarization multiplexed. The output signals from the transceivers are wavelength multiplexed and sent to the RN through an optical fiber. After being distributed to the corresponding ONU, the downstream baseband signal and the UWB signal are converted to electrical signals. A portion of the UWB signal is taped and directed to the FP-LD to perform injection locking of the FP-LD to generate a clear optical carrier for upstream data transmission. The upstream UWB and baseband signals

are also polarization multiplexed. Therefore, a symmetric UWB over WDM-PON is implemented.

To evaluate the performance of injection locking of the FP-LD, a comparative study is performed in which the injection locking using a baseband and a UWB downstream signal is considered. For both signals having an identical optical injection power and identical electrical modulation power, injection locking using a UWB signal shows a clear advantage over the use of a baseband signal. The proposed wavelength reuse scheme for the UWB over WDM-PON system has the following advantage. When the UWB signal and the baseband signal have the same injected optical power, the UWB signal can have a higher electrical modulation power than that of the baseband signal, without obvious negative impact on the performance of the upstream signal. This in turn contributes to a better receiver sensitivity of the downstream UWB service. It is true that there is a trade-off between the ERs of the downstream and upstream signals for the case of both UWB and baseband injected signals; however, the utilization of the UWB signal as the injected signal enables the system with a higher tolerance against the power penalty introduced by a relatively higher ER of the downstream signal. Therefore, better performances for both downstream and upstream services of the proposed UWB over WDM-PON can be obtained thanks to this property.

A bidirectional point-to-point transmission of 1.25 Gb/s UWB signal and 10 Gb/s baseband signal over 25-km SMF is experimentally demonstrated. The performance including the eye diagrams, the BERs and the power budget is evaluated. An error free transmission of both downstream and upstream services over a 25-km SMF is achieved. The power penalties due to the wavelength reuse and the polarization multiplexing are measured to be as low as 0.2 dB and 0.3 dB, respectively.

4.2 Design of the UWB over WDM-PON

In this section, a detailed principle description of the proposed UWBoF system is given. The system architecture is introduced and illustrated. A theoretical investigation is performed in which the injection locking using a baseband and a UWB downstream signal is considered. The theoretical basis for the UWB signal injection locking scheme is built.

4.2.1 System architecture

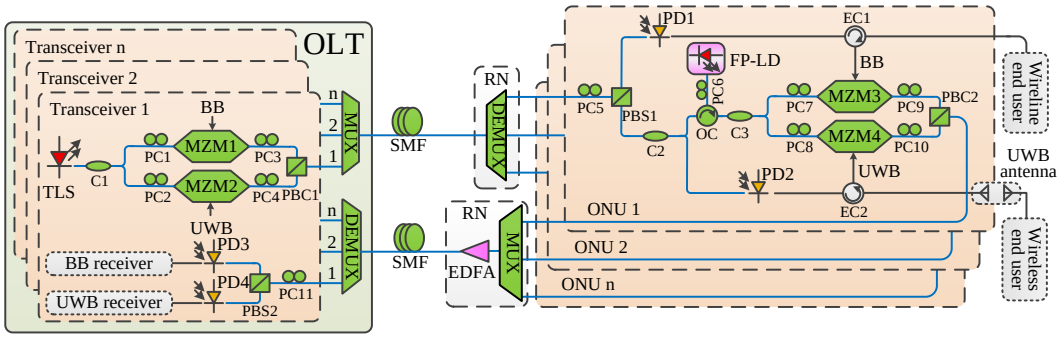

Fig. 4.1. The proposed UWB over WDM-PON architecture with wavelength reuse based on injection locking of an FP-LD and polarization multiplexing. BB: baseband.

The schematic of the proposed UWB over WDM-PON based on injection locking of an FP-LD and polarization multiplexing is shown in Fig. 4.1. At a transceiver

in the OLT, a linearly polarized CW light wave emitted from a TLS is equally divided into two portions through a 50/50 coupler (C1). Each portion of the CW light wave is sent to an MZM through a PC. As illustrated in Fig. 4.1, the upper portion of the CW light wave is intensity-modulated by a baseband signal coded in a PRBS pattern at the MZM (MZM1) while the lower portion is modulated by a PRBS UWB signal at MZM2. The two intensity-modulated signals are then polarization multiplexed at a polarization beam combiner (PBC1) through two other PCs. The optical downstream signals from the transceivers are wavelength multiplexed at a WDM MUX and then transmitted to the RN through a length of SMF where they are de-multiplexed by a WDM DEMUX. The downstream optical signals are then distributed to the corresponding ONUs.

At each ONU, the downstream baseband signal and the UWB signal are polarization de-multiplexed at a polarization beam splitter (PBS1), as shown in Fig. 4.1. The baseband signal is then converted into an electrical signal at PD1 and received by the wireline end user. Therefore, the downstream wireline service is implemented. The UWB signal is divided into two parts through a coupler (C2). The lower part is converted into an electrical signal at PD2 and radiate to the free space through a UWB antenna. The wireless UWB signal can be received by the wireless end user through another UWB antenna. The upper part of the optical

UWB signal is applied to an FP-LD through an OC and a PC for injection locking. A clear optical carrier is generated at the output of the FP-LD and is used for upstream signal modulation. Similar to that of the downstream signal, the upstream signal consists of a baseband signal and a UWB signal. The clear optical carrier is equally divided into two portions through a coupler (C3) and sent to two MZMs (MZM3 and MZM4), at which the optical carriers are modulated by the upstream baseband and UWB signals, as shown in Fig. 4.1. The upstream baseband signal and UWB signal are polarization multiplexed at PBC2, wavelength multiplexed at a MUX, amplified by an EDFA at the RN, and sent to the OLT through a length of SMF. At the OLT, a DEMUX is utilized to de-multiplex the upstream optical signals and send them to the corresponding transceivers. At each transceiver, the optical upstream signal is polarization de-multiplexed through a PC (PC11) and a PBS (PBS2). The polarization de-multiplexed baseband signal and UWB signal are then converted into electrical signals and detected by the corresponding receivers. Consequently, the simultaneous provision of the upstream wireline and wireless services is realized.

4.2.2 Theoretical investigation of the injection locking of an FP-LD

The downstream signal consists of two polarization multiplexed signals, the baseband and the UWB signals. To evaluate the injection locking performance,

we first set the optical powers of the UWB and baseband signals identical. The electrical modulation powers of both signals are also kept identical, but can be tuned at different power levels during the injection locking process.

Mathematically, an amplitude modulated optical signal can be expressed as

$$E_1(t) = A\left[1+\beta s(t)\right]\sin(\omega_s t), \tag{4-1}$$

where A is the amplitude of the optical carrier, β is the amplitude modulation index, $s(t)$ is the normalized electrical UWB or baseband modulation signal, ω_s is the angular frequency of the optical carrier.

The optical signal is injected into the FP-LD and would experience the FP etalon effect in the FP cavity. When the wavelength of the optical carrier is located at one of the transmission peaks of the FP cavity, the FP cavity works as a low pass filter. The high frequency components of the injected signal are filtered out. By considering the FP etalon effect, the optical signal at the output of the cavity can be rewritten as

$$E_2(t) = F^{-1}\left\{F\left[E_1(t)\right]\cdot H(f)\right\}, \tag{4-2}$$

where F and F^{-1} denote the Fourier transform and the inverse Fourier transform, respectively, $H(f)$ is the transfer function of the FP cavity.

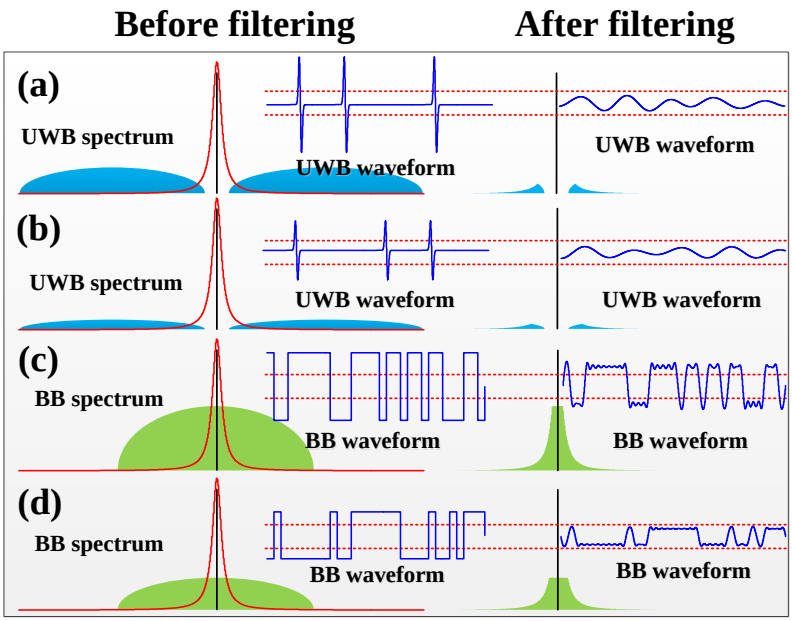

Fig. 4.2. Illustration of the impact of the FP etalon effect on the injected optical UWB and baseband signals.

Fig. 4.2 illustrates the impact of the FP etalon effect on the injected optical UWB and baseband signals. The powers of the electrical modulation signals are varied to show the results corresponding to different modulation depths. The red solid line shows the transmission peak of the target mode in the cavity. From Fig. 4.2(a) and (b), we can see that the UWB signal has most of its power filtered out since most of the frequency components are located at higher frequencies. After

filtering, only some weak lower frequency components remain and the temporal waveform is converted into a quasi-baseband signal with the peak-to-peak amplitude value greatly reduced. When the modulation power increases, the waveform of the filtered signal has small changes, since most of the UWB frequency components are blocked. Therefore, the peak-to-peak amplitude value of the filtered UWB signal is not significantly impacted by the increase of the electrical modulation power. For the baseband signal, shown in Fig. 4.2(c) and (d), since most of the power of the baseband signal is located at the DC and low frequency region, a large proportion of the baseband signal power remains after filtering. When the electrical modulation power increases, the peak-to-peak amplitude of the filtered signal also increases. Therefore, the power of the filtered baseband signal increases significantly with the increase of the modulation depth. It should be noted that, an FP cavity with high reflectivity at both the front and rear facets has stronger filtering effect than that of an anti-reflection FP cavity whose front facet reflectivity can be as low as 1%. With a high reflectivity at both facets, the 3-dB bandwidth of the transfer function of the FP cavity is much narrower. This in turn improves the filtering effect of the cavity. Both of the filtered UWB and baseband signal will be less sensitive to the electrical modulation power.

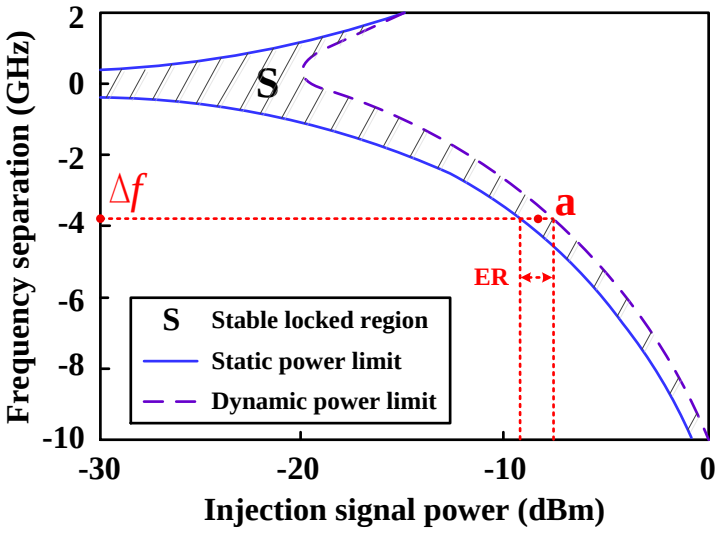

Fig. 4.3. Injection locking of a semiconductor laser [92]. The output optical power of the semiconductor laser is assumed to be 0 dBm.

For a semiconductor laser with a given output power, injection locking of the laser is determined by the injection power and the frequency separation, $\Delta f = f_s - f_i$, where f_s is injection wavelength and f_i is the free running wavelength. However, a strong injection power may lead to relaxation oscillation, thus the injection power should not be too large. To ensure stable injection locking, the injection power must be confined in a region determined by the smallest injection power required to ensure effective injection locking (static power limit) and the maximum injection power limited due to the relaxation oscillation (dynamic power limit) [92]. The static and dynamic power limits can be obtained through finding the stationary solutions of the rate equations of the injection locking system [93, 94]. Fig. 4.3 shows the relationship between the injection power and the frequency

separation [92]. The solid line gives the region defined by the static power limit. The dashed line defines the border of relaxation oscillation. Stable operation is ensured if the injection power and the injection wavelength are within the shadowed region.

As can be seen in Fig. 4.3, the locking wavelength is shifted toward a longer wavelength when the injected power increases (the area formed by the two solid lines is not symmetrical with respect to the zero frequency separation). This is due to the dependence of the refractive index on the carrier density in the cavity active region [95]. For a given frequency separation, there exists an interval of the injection power. This interval set the limit for the minimum and maximum powers of the injection signal, corresponding to the peak-to-peak value or the ER of the injected light. For a different frequency separation, different ER is required. Point *a* in Fig. 4.3 marks the average optical power of the injected signal for a given frequency separation. Mathematically, the power of the filtered signal is given by $P_2(t) = |E_2(t)|^2$. To achieve stable injection locking, $P_2(t)$ should satisfy $P_{\text{static}} < P_2(t) < P_{\text{dynamic}}$, where P_{static} and P_{dynamic} are the power limits set by the static and dynamic limits at a given frequency separation Δf. This condition also indicates that the input optical signal sent to the FP cavity should have a relatively

low ER, i.e., the modulation depth of the downstream signal should not be too high.

Based on the above analysis, the connection between the acceptable maximum electrical modulation power and the stable injection locking can be established. As is shown in Fig. 4.2, the red dotted line marks the acceptable ER of the injected light. For a UWB signal with different electrical modulation power, the maximum and minimum power of the injected light into the target mode of the FP-LD does not change significantly due to the filtering, as shown in Fig. 4.2(a). For the baseband signal, as the modulation power increases, the ER of the filtered signal increases more rapidly than that of the UWB signal, and would exceed the ER limit, as shown in Fig. 4.2(c). Therefore, when the UWB and baseband signal have an identical modulation power, the UWB signal can achieve more stable injection locking as the electrical modulation power increases. The utilization of the UWB signal for injection locking enables the downstream signal to have a higher modulation depth without a severely negative impact on the performance on the upstream service, thus would significantly improve the downstream service performance as well. Through the analysis and comparison, the conclusion is notable: with the same electrical modulation power, the UWB signal is much more suitable for injection locking to generate a clear optical carrier for upstream

data transmission. To achieve the same result as the UWB signal, the modulation power of the baseband signal has to be largely reduced. This would in turn lead to worse receiver sensitivities for the downstream service.

Note that the polarization variations during the optical transmission will have impact on the performance of the system. Similar to the condition in Chapter 3, a solution is to use a polarization stabilizer at the receiver. The use of a polarization stabilizer to compensate for the polarization fluctuations has been proposed and employed in polarization-multiplexed transmission systems [103]. In our proposed system, polarization stabilizers should be placed at the BS and the CS right after the fiber transmission link.

4.3 Experiment

In this section, the experimental setup and the results of the conducted verification experiment is shown.

4.3.1 Experimental setup

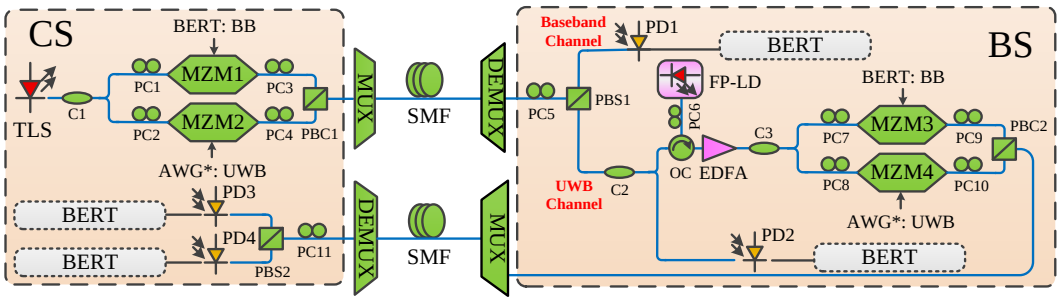

Fig. 4.4. Experimental setup of the proposed wavelength reused UWB over WDM-PON system.

The proposed wavelength reuse scheme in a UWB over WDM-PON system is experimentally demonstrated. The experimental setup is shown in Fig. 4.4. At the CS, a CW light wave at 1553.079 nm from a TLS is equally divided into two parts, and intensity-modulated at two MZM1 and MZM2 by a baseband signal and a UWB signal, respectively. The baseband signal is a 10 Gb/s PRBS non-return-to-zero (NRZ) signal, generated by a BERT (Agilent 4901B); the UWB signal is a 1.25 Gb/s PRBS BPM UWB signal, generated by an arbitrary

waveform generator (AWG*, Tektronix AWG 7102). The polarization states of the two intensity-modulated signals are adjusted by two PCs to make them orthogonally polarized and aligned with the principal axes of a polarization beam combiner (PBC1). The polarization multiplexed downstream signal is then transmitted through a 25-km SMF (Corning SM28) to the BS.

At the BS, the downstream optical signal is sent to a polarization beam splitter (PBS1) via a PC (PC5), to make the signal polarization de-multiplexed. The baseband signal is sent to the upper channel, which is detected by a PD (PD1) (Model 1414, 25 GHz IR Photodetector, New Focus) with the BER measured by a BERT. In the lower channel, the polarization de-multiplexed UWB signal is equally divided into two parts. The lower part is detected by a PD (PD2) (Model 1414, 25 GHz IR Photodetector, New Focus) with the BER performance evaluated by a BERT. The upper part of the optical UWB signal is sent to the FP-LD (Thorlabs S1FC1550) through the OC and PC6 to injection lock one of the longitudinal modes. The FP-LD has a threshold current of about 40 mA and is biased at 60 mA to work at the lasing mode. At the output of the FP-LD, a clear optical carrier is generated. An EDFA is then used to amplify the generated optical carrier. The EDFA can be eliminated if an FP-LD with a higher output power is utilized. The generated optical carrier is then used for upstream data

modulation and transmission. The upstream signals are a 10 Gb/s NRZ baseband signal and a 1.25 Gb/s OOK UWB signal, generated by a BERT and an AWG*, respectively. Similar to the situation for the downstream service, the optical carrier is equally divided into two parts and each is intensity-modulated by an upstream signal at an MZM. The two intensity-modulated signals are polarization multiplexed at PBC2. The upstream optical signal is sent to a MUX and then transmitted back to the CS through a 25-km SMF. After being distributed to the CS by the DEMUX, the upstream optical signal is polarization de-multiplexed at PBS2. The baseband signal and the UWB signal are then detected by two PDs (Model 1414, 25 GHz IR Photodetector, New Focus) and evaluated by the BERTs to measure the BER performance. Therefore, the symmetric wavelength reused UWB over WDM-PON system is implemented.

4.3.2 Experimental results

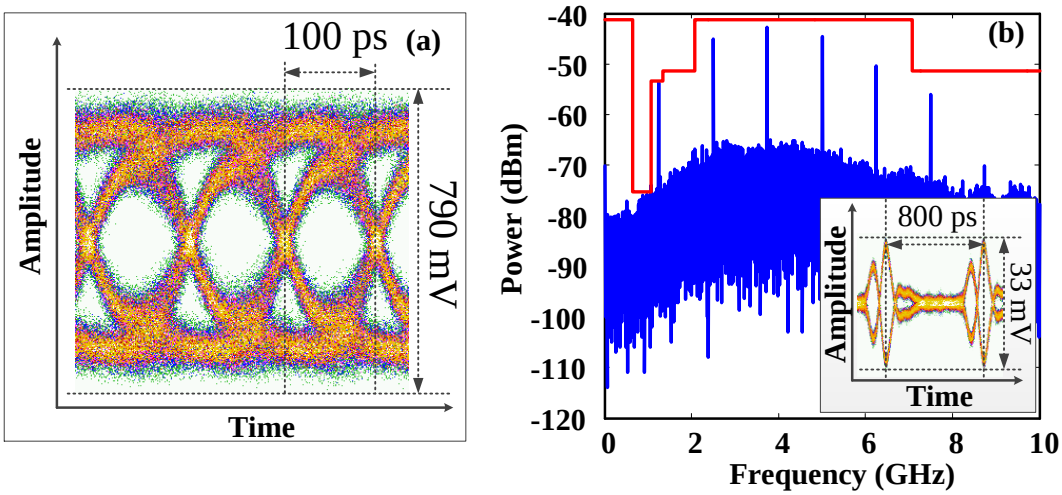

Fig. 4.5. (a) Measured eye diagram of the received downstream baseband signal and (b) measured electrical spectrum and eye diagram of the received downstream UWB signal.

The eye diagrams of the received downstream baseband signal and UWB signal are measured and shown in Fig. 4.5. As can be seen, the eyes of the received downstream baseband signal and the UWB signal are widely opened. The electrical spectrum of the received downstream UWB signal is also measured; the PSD of the UWB signal meets the FCC spectrum mask for indoor wireless communication.

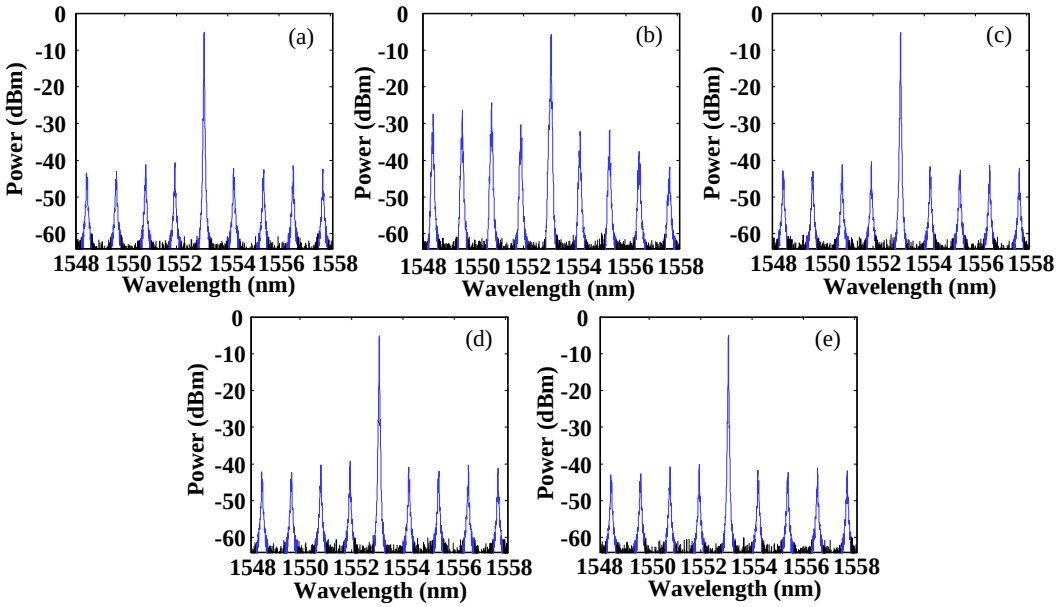

Fig. 4.6. Measured optical spectrums of the output optical carrier of the FP-LD when the following optical signals are injected: (a) clear optical carrier; (b) 5 Gb/s baseband signal with Pmax; (c) 5 Gb/s baseband signal with Pmin; (d) 1.25 Gb/s UWB signal with Pmax; (e) 1.25 Gb/s UWB signal with Pmin; Pmax: maximum modulation power; Pmin: minimum modulation power.

A comparison experiment using the baseband signal and the UWB signal for injection locking is conducted. As analyzed in Chapter 4.2.2, the modulation powers of the both signals are set identical. The injection locking results are given in Fig. 4.6. Fig. 6(a) shows the injection locking using a clear optical carrier, which is used as a reference. Fig. 4.6(b) and (c) shows the injection locking using a baseband signal with two different electrical modulation powers. It is clearly seen that when the input modulation voltage increases, the injection locking

performance becomes deteriorative. The side mode suppression ratio reduces from 35 dB to 19 dB. Fig. 4.6(d) and (e) shows the injection locking using a UWB signal with again two different electrical modulation powers. It is clearly seen that the FP-LD is well injection locked for the UWB signal with two different modulation powers. The side mode suppression ratio is kept at 35 dB when the modulation power is increased. The experimental result confirms that the UWB signal is more suitable for injection locking to generate a clear optical carrier. For a baseband signal, injection locking can only be achieved when the electrical modulation power is low; when the electrical modulation power increases, the injection locking is severely deteriorated.

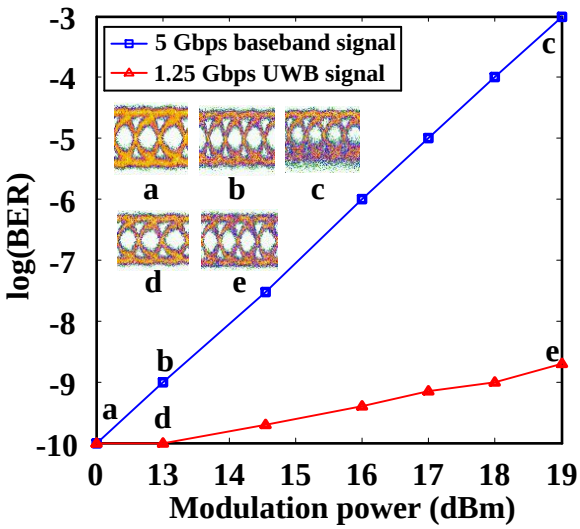

Fig. 4.7. Measured BER and the eye diagrams of a 10 Gb/s upstream baseband signal for an optical carrier from the FP-LD when the input injection signal is an optical baseband signal and an optical UWB signal at different electrical modulation power.

The BER performance and the eye diagrams of a 10 Gb/s upstream baseband signal carried by the reused optical carrier from the FP-LD are measured when the input injection signal is an optical baseband signal and an optical UWB signal at different electrical modulation power. Fig. 4.7 shows the experimental results. From Fig. 4.7 we can see that the BER performance is superior when the injection signal is a UWB signal. When the electrical modulation power is 19 dBm, the upstream signal can maintain error free transmission when the injection signal is a UWB signal with a BER of 10^{-9}, but when the injection signal is a baseband signal, the BER is 10^{-3}. The definition of error free transmission here is identical to that in Chapter 3. The eye diagrams for the two different injection signals are also shown. It is clearly seen the eye diagrams are kept widely open when the input injection signal is a UWB signal at different power levels. The eye diagram is closed when the input injection signal is a baseband signal, especially at high electrical modulation power levels. This result again confirms that the use of a UWB signal as an injection signal provides better performance for upstream signal transmission. When a baseband signal is utilized for injection locking, the upstream service is sensitive to the downstream modulation depth. Through the comparison, the superior properties of UWB signal in the proposed system compared with the baseband signal are verified.

Since the use of a UWB signal for injection lock will provide a better performance, the system will employ the downstream UWB signal as an injection signal for wavelength reuse. The performance of the entire system is then evaluated.

First, the BERs of the downstream and upstream baseband signals are measured, with the results shown in Fig. 4.8. The eye diagrams of the received upstream baseband signals are also shown in Fig. 4.8.

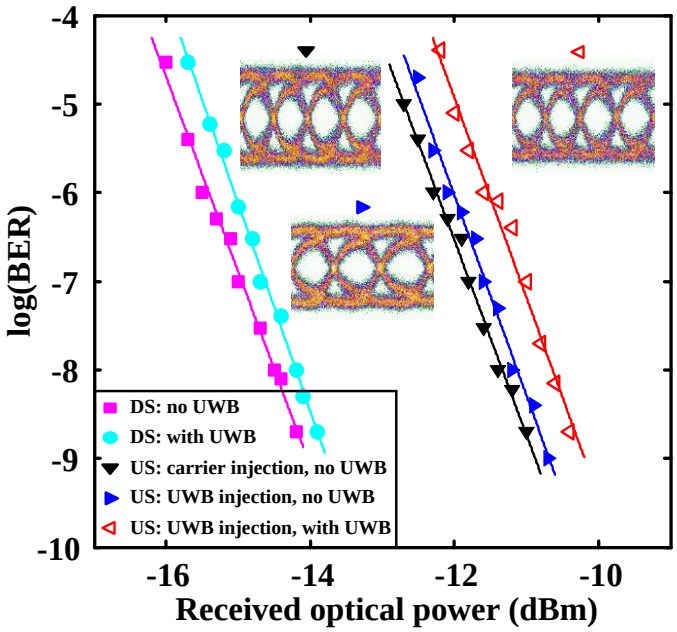

Fig. 4.8. Measured BER of the received downstream and upstream baseband signals. Inset: eye diagrams of the received upstream baseband signals.

The BER of the downstream baseband signal is measured without and with a polarization multiplexed UWB downstream signal to study the performance of the polarization multiplexing of the baseband and UWB signals. As can be seen the co-transmission of a downstream baseband and a downstream UWB signal will introduce a small power penalty of 0.3 dB. The effectiveness of the polarization multiplexing is confirmed.

The BER of the upstream baseband signal is then measured. Three different situations are considered: first, the injection signal is a pure optical carrier; second, the injection signal is a UWB downstream signal with no upstream UWB signal (UWB injection, no UWB); third, the injection signal is UWB downstream signal with a polarization multiplexed upstream UWB signal (UWB injection, with UWB). As can be seen that the power penalties caused by the wavelength reuse and polarization multiplexing are as low as 0.2 dB and 0.3 dB, respectively. The eyes of the upstream signals are also widely open with no obvious deterioration. The good performance of transmission of both the downstream and upstream baseband signals of the proposed system is verified.

Then, the BERs of the downstream and upstream UWB signals are measured, with the results shown in Fig. 4.9. The eye diagrams of the received upstream UWB signals are also shown in Fig. 4.9.

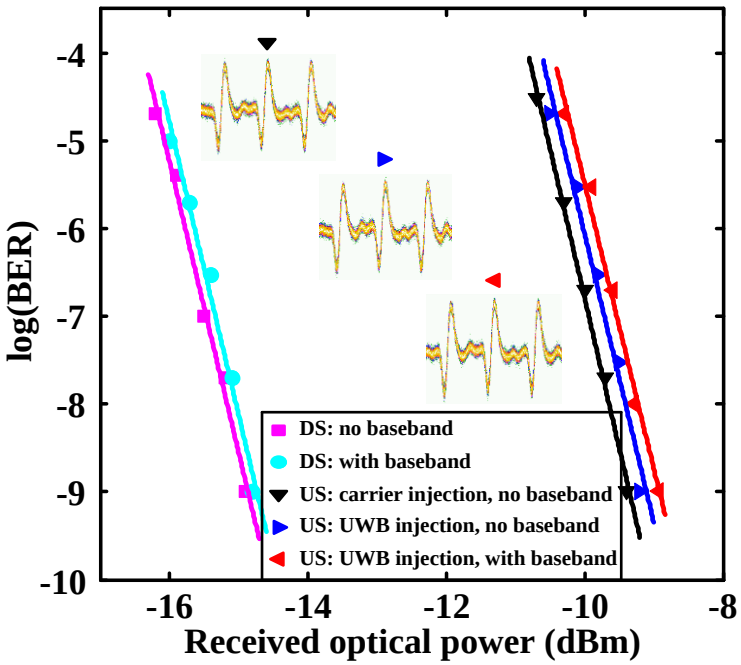

Fig. 4.9. Measured BER of the received downstream and upstream UWB signals. Inset: eye diagrams of the received upstream UWB signals.

Similar to the measurements for the transmission of the baseband signal given in Fig. 4.8, the BER of the downstream UWB signal is measured without and with a polarization multiplexed downstream baseband signal to study the performance of the polarization multiplexing. As can be seen the co-transmission of a downstream

baseband and a downstream UWB signal will introduce a small power penalty of 0.3 dB. The effectiveness of the polarization modulation is again confirmed.

The BER of the upstream UWB signal is then measured. Again, three different situations are considered: first, the injection signal is a pure optical carrier (carrier injection, no baseband); second, the injection signal is a downstream UWB with no upstream baseband signal (UWB injection, no baseband); third, the injection signal is a downstream UWB with a polarization multiplexed upstream baseband signal (UWB injection, with baseband). As can be seen the power penalties caused by the wavelength reuse and polarization multiplexing are both as low as 0.2 dB. The eyes of the upstream UWB signals are also shown in Fig. 4.9, which are widely open. The good performance of transmission of both the downstream and upstream UWB signals of the proposed system is verified.

The receiver sensitivities are also measured. For the downstream BPM UWB signal, the downstream baseband signal, the upstream OOK UWB signal and the upstream baseband signal are -14.8 dBm, -13.9 dBm, -8.9 dBm and -10.4 dBm, respectively. The receiver sensitivity here is defined as the optical power to the receiver required to obtain a BER of 10^{-9} for both the UWB signal and the baseband signal. Note that the receiver sensitivities for the upstream baseband and

UWB signals are worse than those for the downstream signals. This is because the half-wave voltages of the upstream modulators are not high enough, which limits the ERs of the upstream signals. Once the modulators with higher half-wave voltages are utilized, better receiver sensitivities for upstream signals will be attainable.

TABLE III
POWER BUDGET OF THE PROPOSED UWB OVER WDM-PON

Parameters	**Downstream service**		**Upstream service**	
	UWB channel	**Baseband channel**	**UWB channel**	**Baseband channel**
Launch power into fiber link	1 dBm	1 dBm	1 dBm	1 dBm
Fiber link loss	5 dB		5 dB	
Connecter and coupler loss	5 dB	1 dB	1 dB	1 dB
Incident power at receiver	-9 dBm	-5 dBm	-5 dBm	-5 dBm
Receiver sensitivity	-14.8 dBm	-13.9 dBm	-8.9 dBm	-10.4 dBm
CS Minimum launch power: -4.8 dBm			**Power margin: 3.9 dB**	
FP-LD output power: -3 dBm				
EDFA output power: 12 dBm				

The power budget of the proposed UWB over WDM-PON is analyzed, which is summarized in Table III. The output powers of the FP-LD and the EDFA are also

provided. Due to the low output power of the FP-LD, an EDFA is employed at the BS. However, if an FP-LD with a higher output power is used to replace the current FP-LD for the experiment, the EDFA can be eliminated.

4.4 Summary

In this chapter, a wavelength reuse scheme based on injection locking of an FP-LD and polarization multiplexing for a symmetric UWB over WDM-PON was proposed and experimentally demonstrated. The key contribution of the work was the comparative investigation of the performance of injection locking of an FP-LD using a baseband and a UWB signal. It was proved theoretically and experimentally that the use of UWB signal for injection locking will provide better performance than the use of a baseband signal. Thus, the utilization of a downstream UWB signal for wavelength reuse would enable downstream signals to have a higher modulation depth without obviously deteriorating the transmission performance of upstream signals compared with the conventional schemes of injection locking using a baseband signal. Therefore, the proposed UWB over WDM-PON could provide excellent performance for both downstream and upstream services. A bidirectional point-to-point transmission of 1.25 Gb/s UWB signal and 10 Gb/s baseband signal over 25-km SMF was experimentally investigated. The performance including eye diagrams, the BERs and the power budget was evaluated. An error free bidirectional transmission over a 25-km SMF was demonstrated. The power penalties due to wavelength reuse and polarization multiplexing were measured to be as low as 0.2 dB and 0.3 dB respectively.

Chapter 5

Conclusions and Future Works

5.1 Conclusions

In the work of this master's program, the main objective is to realize UWBoF networks with simple and cost effective architecture based on wavelength reuse. In this thesis, two schemes have been proposed and experimentally demonstrated. The objective has been achieved.

In the first experiment, a wavelength reuse scheme based on PM-IM conversion and destructive interferencing in a UWBoF system was proposed and experimentally demonstrated. The key contribution of the technique was the use of the PolM which was operating jointly with the FBG to generate two intensity-modulated signals along two orthogonal SOPs. The combination of the two signals at a polarizer generated a clean optical carrier which was reused for upstream transmission. In addition, since no active elements were employed in the downstream data erasing process, no additional noise and nonlinearity were introduced, the quality of the upstream signal was thus greatly enhanced.

In the second experiment, a wavelength reuse scheme based on injection locking of an FP-LD and polarization multiplexing for a symmetric UWB over WDM-PON was proposed and experimentally demonstrated. The key contribution of the work was the comparative investigation of the performance of injection locking of an FP-LD using a baseband and a UWB signal. It was theoretically explained and experimentally demonstrated that the use of UWB signal for injection locking could provide better performance than a baseband signal. Thus, the utilization of a downstream UWB signal for wavelength reuse would enable downstream signals to have a higher modulation depth without obviously deteriorating the transmission performance of upstream signals compared with the conventional schemes of injection locking using a baseband signal. Therefore, the proposed UWB over WDM-PON could provide excellent performance for both downstream and upstream services.

5.2 Future works

Wavelength reuse has been regarded as an effective and promising technique to realize a colorless ONU in a WDM-PON. In this thesis, two wavelength reuse schemes to achieve UWBoF networks were proposed and demonstrated. The work in this thesis can be further developed from the following aspects.

1) In the first wavelength reuse scheme, the receiver sensitivity of the downstream signal is worse than that of the upstream signal; this is because the downstream UWB signal generation is based on PM-IM conversion at a frequency discriminator, where the effective modulation depth of the downstream signal is lower than that of a regular intensity-modulated one. For PM-IM conversion based UWB generation schemes, a way to improve the receiver sensitivity is to design an FBG with steeper slope at the linear region of the magnitude reflection spectrum, where the PM-IM conversion efficiency is higher.

2) In the second wavelength reuse scheme, although it is demonstrated that the use of a UWB signal as injection signal to injection lock the FP-LD is better than a baseband signal, there still exists a tradeoff between the ERs of the downstream signal and the upstream signal performance. An alternative way to further eliminate such tradeoff should be based on the following aspects: first, use an

FP-LD with higher reflectivity at both the front and the rear mirrors of the cavity to increase the finesse of the FP-LD based filter; second, use a pre-filtered UWB signal as the downstream modulation signal, which has weaker power at the lower frequency band. The modification from this two aspects would lead to a higher FP etalon effect on the injected UWB signal and a clearer optical carrier at the output of the FP-LD.

REFERENCES

[1] G. R. Aiello and G. D. Rogerson, "Ultra-wideband wireless systems," *IEEE Microw. Mag.*, vol. 4, no. 2, pp. 36-47, Jun. 2003.

[2] S. Pan and J. Yao, "IR-UWB-over-fiber systems compatible with WDM-PON networks," *J. Lightw. Technol.*, vol. 29, no. 20, pp. 3025-3034, Oct. 2011.

[3] D. Porcino and W. Hirt, "Ultra-wideband radio technology: Potential and challenges ahead," *IEEE Commun. Mag.*, vol. 41, no. 7, pp. 66-74, Jul. 2003.

[4] M. Ghavami, L. B. Michael, and R. Kohno, *Ultra Wideband Signals and Systems in Communication Engineering.* West Sussex, U.K.: Wiley, 2004.

[5] I. Oppermann, M. Hämäläinen, and J. Iinatti, *UWB Theory and Applications.* Chichester, U.K.: Wiley, 2004.

[6] J. P. Yao, "Photonics for ultrawideband communications," *IEEE Microw. Mag.*, vol. 10, no. 4, pp. 82-95, Jun. 2009.

[7] A. G. Yarovoy, L. P. Ligthart, J. Matuzas, and B. Levitas, "UWB radar for human being detection," *IEEE Aerosp. Electron. Syst. Mag.*, vol. 21, no. 3, pp. 10-14, Mar. 2006.

[8] E. Staderini, "UWB radars in medicine," *IEEE Aerosp. Electron. Syst. Mag.*, vol. 17, no. 1, pp. 13-18, Jan. 2002.

[9] M. Y. W. Chia, S. W. Leong, C. K. Sim, and K. M. Chan, "Through-wall UWB radar operating within FCC's mask for sensing heart beat and breathing rate," in *Proc. 35th Eur. Microw. Conf.*, Paris, France, pp. 267-270, Oct. 2005.

[10] R. Kapoor, A. Banerjee, G. A. Tsihrintzis, and N. Nandhakumar, "UWB radar detection of targets in foliage using alpha-stable clutter models," *IEEE Trans. Aerosp. Electron. Syst.*, vol. 35, no. 3, pp. 819-834, Jul. 1999.

[11] R. Xu, Y. Jin, and C. Nguyen, "Power-efficient switching-based CMOS UWB transmitters for UWB communications and radar systems," *IEEE Trans. Microw. Theory Tech.*, vol. 54, no. 8, pp. 3271-3277, Aug. 2006.

[12] I. Immoreev and T.-H. Tao, "UWB radar for patient monitoring," *IEEE Aerosp. Electron. Syst. Mag.*, vol. 23, no. 11, pp. 11-18, Nov. 2008.

[13] J. D. Taylor, *Ultra-Wideband Radar Technology*. New York: CRC Press, 2001.

[14] S. Kidera, T. Sakamoto, and T. Sato, "Accurate UWB radar 3-D imaging algorithm for complex boundary without range points connections," *IEEE Trans. Geosci. Remote Sens.*, vol. 48, no. 4, pp. 1993-2004, Apr. 2010.

[15] M. G. M. Hussain, "Ultra-wideband impulse radar—An overview of the principles," *IEEE Aerosp. Electron. Syst. Mag.*, vol. 31, no. 9, pp. 9-14, Sep. 1998.

[16] C. Le, T. Dogaru, L. Nguyen, and M. A. Ressler, "Ultrawideband (UWB) radar imaging of building interior: Measurements and predictions," *IEEE Trans. Geosci. Remote Sens.*, vol. 47, no. 5, pp. 1409-1420, May 2009.

[17] G. Ossberger, T. Buchegger, E. Schimback, A. Stelzer, and R. Weigel, "Non-invasive respiratory movement detection and monitoring of hidden humans using ultra wideband pulse radar," in *Proc. Int. Workshop Ultrawideband Syst. Technol.*, pp. 395-399, May 2004.

[18] C. M. Zhang, M. J. Kuhn, B. C. Merkl, A. E. Fathy, and M. R. Mahfouz, "Real-Time noncoherent UWB positioning radar with millimeter range accuracy: Theory and experiment," *IEEE Trans. Microw. Theory Tech.*, vol. 58, no. 1, pp. 9-20, Jan. 2010.

[19] Fed. Commun. Commission, *Revision of Part 15 of the Commission's Rules Regarding Ultra-Wideband Transmission Systems*, Apr. 2002. Tech. Rep., ET-Docket 98-153, FCC02-48.

[20] J. P. Yao, F. Zeng, and Q. Wang, "Photonic generation of ultrawideband signals," *J. Lightw. Technol.*, vol. 25, no. 11, pp. 3219-3235, Nov. 2007.

[21] K. Siwiak and D. McKeown, *Ultra-Wideband Radio Technology*. Chichester, U.K.: Wiley, 2004.

[22] L. Q. Yang and G. B. Giannakis, “Ultra-wideband communications: An idea whose time has come,” *IEEE Signal Process. Mag.*, vol. 21, no. 6, pp. 26-54, Nov. 2004.

[23] C. R. Nassar, F. Zhu, and Z. Wu, “Direct sequence spreading UWB systems: Frequency domain processing for enhanced performance and throughput,” in *Proc. IEEE Int. Conf. Commun.*, vol. 3, pp. 2180-2186, May 2003.

[24] J. Balakrishnan, A. Batra, and A. Dabak, “A multi-band OFDM system for UWB communication,” in *Proc. IEEE Conf. Ultra Wideband Syst. Technol.*, pp. 354-358, Nov. 2003.

[25] S. Pan and J. Yao, “A UWB over fiber system compatible with WDM-PON architecture,” *IEEE Photon. Technol. Lett.*, vol. 22, no. 20, pp. 1500-1502, Oct. 2010.

[26] K. Grobe and J. P. Elbers, “PON in adolescence: From TDMA to WDM-PON,” *IEEE Commun. Mag.*, vol. 46, no. 1, pp. 26-34, Jan. 2008.

[27] S. Pan and J. Yao, “Simultaneous provision of UWB and wired services in a WDM-PON network using a centralized light source,” *IEEE Photon. J.*, vol. 2, no. 5, pp. 711-718, Oct. 2010.

[28] K. Kim, “On the evolution of PON-based FTTH solutions,” *Inform. Sci.*, vol. 149/1 – 2, pp. 21-30, Jan. 2003.

[29] G.-K. Chang, A. Chowdhury, Z. Jia, H.-C. Chien, M.-F. Huang, J. Yu, and G. Ellinas, "Key technologies of WDM-PON for future converged optical broadband access networks," *J. Opt. Commun. Netw.*, vol. 1, pp. C30-C50, Sep. 2009.

[30] A. Banerjee, Y. Park, F. Clarke, H. Song, S. Yang, G. Kramer, K. Kim, and B. Mukherjee, "Wavelength-division-multiplexed passive optical network (WDM-PON) technologies for broadband access: A review," *OSA J. Opt. Netw.*, vol. 4, no. 11, pp. 737-758, Nov. 2005.

[31] K. Prince, J. B. Jensen, A. Caballero, X. B. Yu, T. B. Gibbon, D. Zibar, N. Guerrero, A. V. Osadchiy, and I. T. Monroy, "Converged wireline and wireless access over a 78-km deployed fiber long-reach WDM PON," *IEEE Photon. Technol. Lett.*, vol. 21, no. 17, pp. 1274-1276, Sep. 2009.

[32] S. Pan and J. Yao, "Provision of IR-UWB wireless and baseband wired services over a WDM-PON," *Opt. Express*, vol. 19, no. 26, pp. B209-B217, Dec. 2011.

[33] Z. Dong, J. Lu, Y. Pi, X. Lei, L. Chen, and J. Yu, "Optical millimeter-wave signal generation and wavelength reuse for upstream connection in radio-over-fiber systems," *J. Opt. Netw.*, vol. 7, no. 8, pp. 736-743, Aug. 2008.

[34] F. Zeng and J. P. Yao, "Ultrawideband impulse radio signal generation using a high-speed electrooptic phase modulator and a fiber-Bragg-grating-based frequency discriminator," *IEEE Photon. Technol. Lett.*, vol. 18, no. 19, pp. 2062-2064, Oct. 2006.

[35] F. Zeng, Q. Wang, and J. P. Yao, "All-optical UWB impulse generation based on cross phase modulation and frequency discrimination," *Electron. Lett.*, vol. 43, no. 2, pp. 119-121, Jan. 2007.

[36] F. Zeng and J. P. Yao, "An approach to ultra-wideband pulse generation and distribution over optical fiber," *IEEE Photon. Technol. Lett.*, vol. 18, no. 7, pp. 823-825, Mar. 2006.

[37] Q. Wang and J. P. Yao, "Optically switchable UWB monocycle and doublet generation using a reconfigurable photonic microwave delay-line filter," *Opt. Express*, vol. 15, no. 22, pp. 14667-14672, Oct. 2007.

[38] H. Mu and J. P. Yao, "Polarity- and shape-switchable UWB pulse generation based on a photonic microwave delay-line filter with a negative tap coefficient," *IEEE Photon. Technol. Lett.*, vol. 21, no. 17, pp. 1253-1255, Sep. 2009.

[39] I. Lin, J. D. McKinney, and A. M. Weiner, "Photonic synthesis of broadband microwave arbitrary waveforms applicable to ultrawideband communication," *IEEE Microw. Wireless Compon. Lett.*, vol. 15, no. 4, pp. 226-228, Apr. 2005.

[40] C. Wang, F. Zeng, and J. P. Yao, "All-fiber ultrawideband pulse generation based on spectral shaping and dispersion-induced frequency-to-time conversion," *IEEE Photon. Technol. Lett.*, vol. 19, no. 3, pp. 137-139, Feb. 2007.

[41] Z. Jia, J. Yu, G. Ellinas, and G.-K. Chang, "Key enabling technologies for optical-wireless networks: Optical millimeter-wave generation, wavelength reuse and architecture," *J. Lightw. Technol.*, vol. 25, no. 11, pp. 3452-3471, Nov. 2007.

[42] F. Payoux, P. Chanclou, and N. Genay, "WDM-PON with colourless ONUs," in *Proc. Opt. Fiber Conf.*, Anaheim, CA, paper OTuG5, Mar. 2007.

[43] R. Lin, "Next generation PON in emerging networks," in *Proc. OFC/NFOEC*, San Diego, CA, USA, Feb. 2008.

[44] J.-I. Kani, "Enabling technologies for future scalable and flexible WDM-PON and WDM/TDM-PON systems," *IEEE J. Sel. Topics Quantum Electron.*, vol. 16, no. 5, pp. 1290-1297, Sep. /Oct. 2010.

[45] E. Wong, "Next-generation broadband access networks and technologies," *J. Lightw. Technol.*, vol. 30, no. 4, pp. 597-608, Feb. 2012.

[46] L. Y. Chan, C. K. Chan, D. T. K. Tong, F. Tong, and L. K. Chen, "Upstream traffic transmitter using injection-locked Fabry-Pérot laser diode as modulator

for WDM access networks," *Electron. Lett.*, vol. 38, no. 1, pp. 43-45, Jan. 2002.

[47] W. Hung, C. K. Chan, L. K. Chen, and F. Tong, "An optical network unit for WDM access networks with downstream DPSK and upstream remodulated OOK data using injection-locked FP laser," *IEEE Photon. Technol. Lett.*, vol. 15, no. 10, pp. 1476-1478, Oct. 2003.

[48] F. Xiong, W.-D. Zhong, and H. Kim, "A broadcast-capable WDM-PON based on polarization-sensitive weak-resonant-cavity Fabry-Perot laser diodes," *J. Lightwave Technol.*, vol. 30, no. 3, pp. 355-361, Feb. 2012.

[49] S. M. Lee, K. M. Choi, S. G. Mun, J. H. Moon, and C. H. Lee, "Dense WDM-PON based on wavelength-locked Fabry-Pérot laser diodes," *IEEE Photon. Technol. Lett.*, vol. 17, no. 7, pp. 1579-1581, Jul. 2005.

[50] W. R. Lee, M. Y. Park, S. H. Cho, J. H. Lee, C. Y. Kim, G. Jeong, and B. W. Kim, "Bidirectional WDM-PON based on gain-saturated reflective semiconductor optical amplifiers," *IEEE Photon. Technol. Lett.*, vol. 17, no. 11, pp. 2460-2462, Nov. 2005.

[51] I. Papagiannakis, M. Omella, D. Klonidis, J. A. Lázaro, A. Birbas, J. Kikidas, I. Tomkos, and J. Prat, "Design characteristics for a full-duplex IM/IM bidirectional transmission at 10 Gb/s using low bandwidth RSOA," *J. Lightwave Technol.*, vol. 28, no. 7, pp. 1094-1101, Apr. 2010.

[52] T. Y. Kim and S. K. Han, "Reflective SOA-based bidirectional WDM-PON sharing optical source for up/downlink data and broadcasting transmission," *IEEE Photon. Technol. Lett.*, vol. 18, no. 22, pp. 2350-2352, Nov. 15, 2006.

[53] M. Presi, R. Proietti, K. Prince, G. Contestabile, and E. Ciaramella, "A 80 km reach fully passive WDM-PON based on reflective ONUs," *Opt. Express*, vol. 16, no. 23, pp. 19043-19048, Nov. 2008.

[54] L. Chen, H. Wen, and S. Wen, "A radio-over-fiber system with a novel scheme for millimeter-wave generation and wavelength reuse for up-link connection," *IEEE Photon. Technol. Lett.*, vol. 18, no. 19, pp. 2056-2058, Oct. 2006.

[55] Z. Jia, J. Yu, and G.-K. Chang, "A full-duplex radio-over-fiber system based on optical carrier suppression and reuse," *IEEE Photon. Technol. Lett.*, vol. 18, no. 16, pp. 1726-1728, Aug. 2006.

[56] J. Yu, Z. Jia, T. Wang, and G. K. Chang, "Centralized lightwave radio-over-fiber system with photonic frequency quadrupling for high-frequency millimeter-wave generation," *IEEE Photon. Technol. Lett.*, vol. 19, no. 19, pp. 1499-1501, Oct. 2007.

[57] J. Yu, Z. Jia, T. Wang, and G. K. Chang, "A novel radio-over-fiber configuration using optical phase modulator to generate an optical mm-wave

and centralized lightwave for uplink connection," *IEEE Photon. Technol. Lett.*, vol. 19, no. 3, pp. 140-142, Feb. 2007.

[58] X. Zhang, B. Liu, J. Yao, K. Wu, and R. Kashyap, "A novel millimeter-wave-band radio-over-fiber system with dense wavelength-division multiplexing bus architecture," *IEEE Trans. Microw. Theory Tech.*, vol. 54, no. 2, pt. 2, pp. 929-937, Feb. 2006.

[59] B. L. Dang, M. Garcia Larrode, R. Venkatesha Prasad, I. Niemegeers, and A. M. J. Koonen, "Radio-over-Fiber based architecture for seamless wireless indoor communication in the 60 GHz band," *Comput. Commun.*, vol. 30, pp. 3598-3613, Dec. 2007.

[60] C. Lim, A. Nirmalathas, M. Bakaul, P. Gamage, K.-L. Lee, Y. Yang, D. Novak, and R. Waterhouse, "Fiber-wireless networks and subsystem technologies," *J. Lightw. Technol.*, vol. 28, no. 4, pp. 390-405, Feb. 2010.

[61] J. J. V. Olmos, T. Kuri, and K.-I. Kitayama, "Reconfigurable radio-over-fiber networks multiple-access functionality directly over the optical layer," *J. Lightw. Technol.*, vol. 58, no. 11, pp. 3001-3010, Nov. 2010.

[62] H. Ishida and K. Araki, "Design and analysis of UWB bandpass filter with ring filter," in *IEEE MTT-S Int. Tech. Dig.*, vol. 3, pp. 1307-1310, Jun. 2004.

[63] L. Zhu, S. Sun, and W. Menzel, "Ultra-wideband (UWB) bandpass filters using multiple-mode resonator," *IEEE Microw. Wireless Compon. Lett.*, vol. 15, no. 11, pp. 796-798, Nov. 2005.

[64] H. Ishida and K. Araki, "A design of tunable UWB filters," in *Proc. Int. Workshop Ultra Wideband Systems*, pp. 424-428, May 2004.

[65] A. Saito, H. Harada, and A. Nishikata, "Development of band pass filter for ultra wideband (UWB) communication systems," in *Proc. IEEE Conf. Ultra Wideband Systems Technology*, pp. 76-80, Nov. 2003.

[66] W. P. Lin and J. Y. Chen, "Implementation of a new ultrawide-band impulse system," *IEEE Photon. Technol. Lett.*, vol. 17, no. 11, pp. 2418-2420, Nov. 2005.

[67] J. Han and C. Nguyen, "A new ultra-wideband, ultra-short monocycle pulse generator with reduced ringing," *IEEE Microw. Wireless Compon. Lett.*, vol. 12, no. 6, pp. 206-208, Jun. 2002.

[68] Y. Jeong and S. Jung, "A CMOS impulse generator for UWB wireless communication system," in *Proc. 2004 IEEE Int. Symp. Circuit and Systems*, pp. IV-129-IV-132, May 2004.

[69] E. Zhou, X. Xu, K. S. Lui, and K. K. Y. Wong, "A power-efficient ultra-wideband pulse generator based on multiple PM-IM conversions," *IEEE Photon. Technol. Lett.*, vol. 22, no. 14, pp. 1063-1065, Jul. 2010.

[70] E. Zhou, X. Xu, K. Lui, and K. K. Wong, "High-speed photonic power-efficient ultra-wideband transceiver based on multiple PM-IM conversions," *IEEE Trans. Microw. Theory Tech.*, vol. 58, no. 11, pp. 3344-3351, Nov. 2010.

[71] E. Zhou, X. Xu, K. S. Lui, and K. K. Y. Wong, "Photonic ultrawideband pulse generation with HNL-DSF-based phase and intensity modulator," *IEEE Photon. Technol. Lett.*, vol. 23, no. 7, pp. 396-398, Apr. 2011.

[72] J. J. Dong, X. L. Zhang, J. Xu, D. X. Huang, S. N. Fu, and P. Shum, "Ultrawideband monocycle generation using cross-phase modulation in a semiconductor optical amplifier," *Opt. Lett.*, vol. 32, no. 10, pp. 1223-1225, May, 2007.

[73] F. Zeng and J. P. Yao, "Frequency domain analysis of fiber Bragg grating based phase modulation to intensity modulation conversion," in *Proc. SPIE*, p. 59712B, Sep. 2005.

[74] M. Bolea, J. Mora, B. Ortega, and J. Capmany, "Optical UWB pulse generator using an N tap microwave photonic filter and phase inversion adaptable to different pulse modulation formats," *Opt. Express*, vol. 17, no. 7, pp. 5023-5032, Mar. 2009.

[75] M. Bolea, J. Mora, B. Ortega, and J. Capmany, "Flexible monocycle UWB generation for reconfigurable access networks," *IEEE Photon. Technol. Lett.*, vol. 22, no. 12, pp. 878-880, Jun. 2010.

[76] Q. Wang, F. Zeng, S. Blais, and J. P. Yao, "Optical ultrawideband monocycle pulse generation based on cross-gain modulation in a semiconductor optical amplifier," *Opt. Lett.*, vol. 31, no. 21, pp. 3083-3085, Nov. 2006.

[77] J. Li, B. P. P. Kuo, and K. K. Y. Wong, "Ultra-wideband pulse generation based on cross-gain modulation in fiber optical parametric amplifier," *IEEE Photon. Technol. Lett.*, vol. 21, no. 4, pp. 212-214, Feb. 2009.

[78] S. L. Pan and J. P. Yao, "A photonic UWB generator reconfigurable for multiple modulation formats," *IEEE Photon. Technol. Lett.*, vol. 21, no. 19, pp. 1381-1383, Oct. 2009.

[79] S. L. Pan and J. P. Yao, "Optical generation of polarity- and shape-switchable UWB pulses using an chirped intensity modulator and a first-order asymmetric Mach-Zehnder interferometer," *Opt. Lett.*, vol. 34, no. 9, pp.1312-1314, May 2009.

[80] S. Pan and J. P.Yao, "Switchable UWB pulses generation using a phase modulator and a reconfigurable asymmetric Mach-Zehnder interferometer," *Opt. Lett.*, vol. 34, no. 2, pp. 160-162, Jan. 2009.

[81] M. Abtahi, J. Magné, M. Mirshafiei, L. A. Rusch, and S. LaRochelle, "Generation of power-efficient FCC-compliant UWB waveforms using FBGs: Analysis and experiment," *J. Lightwave Technol.*, vol. 26, no. 5, pp. 628-635, Mar. 2008.

[82] J. D. McKinney, I. S. Lin, and A.M.Weiner, "Shaping the power spectrum of ultra-wideband radio-frequency signals," *IEEE Trans. Microw. Theory Tech.*, vol. 54, no. 12, pp. 4247-4255, Dec. 2006.

[83] M. Abtahi, M. Mirshafiei, J. Magne, L. A. Rusch, and S. LaRochelle, "Ultra-wideband waveform generator based on optical pulse-shaping and FBG tuning," *IEEE Photon. Technol. Lett.*, vol. 20, no. 2, pp. 135-137, Jan. 15, 2008.

[84] X. Yu, T. B. Gibbon, M. Pawlik, S. Blaaberg, and I. T. Monroy, "A photonic ultra-wideband pulse generator based on relaxation oscillations of a semiconductor laser," *Opt. Express*, vol. 17, no. 12, pp. 9680-9687, Jun. 2009.

[85] V. Torres-Company, K. Prince, and I. T. Monroy, "Ultrawideband pulse generation based on overshooting effect in gain-switched semiconductor laser," *IEEE Photon. Technol. Lett.*, vol. 20, no. 15, pp. 1299-1301, Aug. 2008.

[86] T. B. Gibbon, X. Yu, D. Zibar, and I. T. Monroy, "Novel ultra-wideband photonic signal generation and transmission featuring digital signal processing

bit error rate measurements," in *Proc. OFC/NFOEC 2009*, CA, p. OTuB8, Mar. 2009.

[87] T. B. Gibbon, X. B. Yu, R. Gamatham, N. G. Gonzalez, R. Rodes, J. B. Jensen, A. Caballero, and I. T. Monroy, "3.125 Gb/s impulse radio ultra-wideband photonic generation and distribution over a 50 km fiber with wireless transmission," *IEEE Microw. Wireless Compon. Lett.*, vol. 20, no. 2, pp. 127-129, Feb. 2010.

[88] X. Yu, T. B. Gibbon, D. Zibar, and I. T. Monroy, "A novel incoherent scheme for photonic generation of biphase modulated UWB signals," in *Proc. OFC/NFOEC' 09*, p. JWA60, Mar. 2009.

[89] X. Yu, T. B. Gibbon, and I. T. Monroy, "Experimental demonstration of all-optical 781.25-Mb/s binary phase-coded UWB signal generation and transmission," *IEEE Photon. Technol. Lett.*, vol. 21, no. 17, pp. 1235-1237, Sep. 2009.

[90] X. Yu and I. T. Monroy, "Distribution of photonically generated 5 Gbits/s impulse radio ultrawideband signals over fiber," *Opt. Lett.*, vol. 36, no. 6, pp. 810-812, Mar. 2011.

[91] T. B. Gibbon, X. Yu, and I. T. Monroy, "Photonic ultra-wideband 781.25-Mb/s signal generation and transmission incorporating digital signal

processing detection," *IEEE Photon. Technol. Lett.*, vol. 21, no. 15, pp. 1060-1062, Aug. 2009.

[92] S. Yamashita and D. Matsumoto, "Waveform reshaping based on injection locking of a distributed-feedback semiconductor laser," *IEEE Photon. Technol. Lett.*, vol. 12, no. 10, pp. 1388-1390, Oct. 2000.

[93] V. Annovazzi-Lodi, A. Scire, M. Sorel, and S. Donati, "Dynamic behavior and locking of a semiconductor laser subjected to external injection," *IEEE J. Quantum Electron.*, vol. 34, no. 12, pp. 2350-2357, Dec. 1998.

[94] F. Mogensen, H. Olesen, and G. Jacobsen, "Locking conditions and stability properties for a semiconductor lasers with external light injection," *IEEE J. Quantum Electron.*, vol. QE-21, no. 7, pp. 784-793, Jul. 1985.

[95] R. Lang, "Injection locking properties of a semiconductor laser," *IEEE J. Quantum Electron.*, vol. QE-18, no. 6, pp. 976-983, Jun. 1982.

[96] H. Takesue and T. Sugie, "Wavelength channel data rewrite using saturated SOA modulator for WDM networks with centralized light sources," *J. Lightw. Technol.*, vol. 21, no. 11, pp. 2546-2556, Nov. 2003.

[97] J. J. V. Olmos, T. Kuri, and K. -I. Kitayama, "60-GHz-band 155-Mb/s and 1.5-Gb/s baseband time-slotted full-duplex radio-over-fiber access network," *IEEE Photon. Technol. Lett.*, vol. 20, no. 7, pp. 617-619, Apr. 2008.

[98] Y. Tian, Q. J. Chang, and Y. K. Su, "A WDM passive optical network enabling multicasting with color-free ONUs," *Opt. Exp.*, vol. 16, no. 14, pp. 10434-10439, Jul. 2008.

[99] O. Akanbi, J. Yu, and G. K. Chang, "A new scheme for bidirectional WDM-PON using upstream and downstream channels generated by optical carrier suppression and separation technique," *IEEE Photon. Technol. Lett.*, vol. 18, no. 2, pp. 340-342, Jan. 2006.

[100] J. Yu and G.-K. Chang, "A novel technique for optical label and payload generation and multiplexing using optical carrier suppression and separation," *IEEE Photon. Technol. Lett.*, vol. 16, no. 1, pp. 320-322, Jan. 2004.

[101] Q. Wang and J. P. Yao, "An electrically switchable optical ultra-wideband pulse generator," *J. Lightw. Technol.*, vol. 25, no. 11, pp. 3626-3633, Nov. 2007.

[102] Q. Wang and J. P. Yao, "UWB doublet generation using a nonlinearly-biased electro-optic intensity modulator," *Electron. Lett.*, vol. 42, no. 22, pp. 1304-1305, Oct. 2006.

[103] P. Boffi, M. Ferrario, L. Marazzi, P. Martelli, P. Parolari, A. Righetti, R. Siano, and M. Martinelli, "Measurement of PMD tolerance in 40-Gb/s polarization-multiplexed RZ-DQPSK," *Opt. Express*, vol. 16, no. 17, pp. 13398-13404, Aug. 2008.

LIST OF ACRONYMS

A

A/D	analogue-to-digital convertor
AP	access point
Att.	Attenuator
AWG	arrayed waveguide grating
AWG*	arbitrary waveform generator

B

BER	bit error rate
BB	baseband
BERT	bit error rate tester
BS	base station
BPM	bi-phase modulation

C

CCD	charge coupled device
CRC	Communications Research Center
CS	central station
CW	continuous wave

D

DC	direct current
DE	dispersive element
DGD	differential group delay
DFB	distributed feedback
DCF	dispersion compensation fiber
DSP	digital signal processing
DEMUX	de-multiplexer
DAM	dual-arm modulator
DS	downstream

E

EMI	immunity to electromagnetic interference
EPON	Ethernet PON
ER	extinction ratio
EDFA	erbium-doped fiber amplifier
ESA	electrical spectrum analyzer
EC	electrical circulator

F

FBG	Fiber Bragg grating
FSR	increasing free spectral range
FWHM	full-width at half-maximum
FCC	Federal Communications Commission
FTTH	fiber to the home
FP-LD	Fabry-Pérot laser diode

G

GPON Gigabit PON

H

HPF high pass filter

I

IL interleaver

L

LD laser diode
LPF low-pass filter
LO local oscillator

M

MLL mode-locked laser
MLFL mode-locked fiber laser
MZI Mach-Zehnder interferometer
MZM Mach-Zehnder modulator
MUX multiplexer

N

NRZ non-return-to-zero

O

ONU optical network unit
OLT optical line terminal
OC optical circulator
OOK on-off-keying

P

PC polarization controller
PD photodetector
PSD power spectral density
PON passive optical network
PM phase modulator
PM-IM phase modulation to intensity modulation
PolM polarization modulator
PDA personal digital assistant
PRBS pseudorandom bit sequence
PMF polarization-maintaining fiber
P-t-P point-to-point
PBC polarization beam coupler
PBS polarization beam splitter
Pol polarizer

R

RSOA reflective semiconductor optical amplifier
RF radio-frequency
Rx receiver
RN remote node
RBW resolution bandwidth

S

SOP state of polarization
SMF single-mode fiber
SNR signal to noise ratio

T

TDMA	time-division multiple access work
TOF	tunable optical filter
TE	transverse electric
TM	transverse magnetic
TLS	tunable laser source

U

UWB	ultra-wideband
US	upstream

W

WDM	wavelength division multiplexing
WLAN	wireless local-area network
WPAN	wireless personal-area network

X

XGM	cross gain modulation

LIST OF FIGURES

Number *Page*